

THE CHEMISTRY OF POPULATION III SUPERNOVA EJECTA. I. FORMATION OF MOLECULES IN THE EARLY UNIVERSE

ISABELLE CHERCHNEFF¹ AND ELI DWEK²

¹ Departement Physik, Universität Basel, CH-4056 Basel, Switzerland; isabelle.cherchneff@unibas.ch

² Observational Cosmology Laboratory, Code 665, NASA Goddard Space Flight Center, Greenbelt, MD 20771, USA; eli.dwek@nasa.gov
Received 2009 April 21; accepted 2009 July 23; published 2009 August 31

ABSTRACT

We study the formation and destruction of molecules in the ejecta of Population III supernovae (SNe) using a chemical kinetic approach to follow the evolution of molecular abundances from day 100 to day 1000 after explosion. The chemical species included in the study range from simple diatomic molecules to more complex dust precursor species. All relevant molecule formation and destruction processes that are unique to the SN environment are considered. Our work focuses on zero-metallicity progenitors with masses of 20, 170, and 270 M_{\odot} , and we study the effect of different levels of heavy element mixing and the inward diffusion of hydrogen and helium on the ejecta chemistry. We show that the ejecta chemistry does not reach a steady state within the relevant timespan (~ 3 yr) for molecule formation, thus invalidating previous results relying on this assumption. The primary species formed in the harsh SN environment are O_2 , CO, SiS, and SO. The SiO, formed as early as 200 days after explosion, is rapidly depleted by the formation of silica molecular precursors in the ejecta. The rapid conversion of CO to C_2 and its thermal fractionation at temperatures above 5000 K allow for the formation of carbon chains in the oxygen-rich zone of the unmixed models, providing an important pathway for the formation of carbon dust in hot environments where the C/O ratio is less than 1. We show that the fully mixed ejecta of a 170 M_{\odot} progenitor synthesizes 11.3 M_{\odot} of molecules, whereas 20 M_{\odot} and 270 M_{\odot} progenitors produce 0.78 M_{\odot} and 3.2 M_{\odot} of molecules, respectively. The admixing of 10% of hydrogen into the fully mixed ejecta of the 170 M_{\odot} progenitor increases its molecular yield to $\sim 47 M_{\odot}$. The unmixed ejecta of a 170 M_{\odot} progenitor SN without hydrogen penetration synthesizes $\sim 37 M_{\odot}$ of molecules, whereas its 20 M_{\odot} counterpart produces $\sim 1.2 M_{\odot}$. This smaller efficiency at forming molecules is due to the large fraction of He^+ in the outer mass zone of the ejecta. Finally, we discuss the cosmological implication of molecule formation by Pop III SNe in the early universe.

Key words: astrochemistry – early universe – molecular processes – supernovae: general

1. INTRODUCTION

Large column densities of dust are required to explain the reddening of background quasars and Ly α systems at high redshift ($z > 6$; Pettini et al. 1994; Pei & Fall 1995) and about $2 \times 10^8 M_{\odot}$ of dust is derived from the infrared (IR) spectrum of the hyperluminous galaxy SDSS J1148+5251 at redshift $z = 6.4$ (Bertoldi et al. 2003; Robson et al. 2004; Beelen et al. 2006; Dwek et al. 2007). The origin of such large quantities of dust when the universe was less than 1 Gyr old is still a matter of debate. In the local universe, dust forms in high density and temperature regions encountered in circumstellar environments such as the winds of asymptotic giant branch (AGB) stars and supergiant stars, the colliding winds of Wolf–Rayet stars, and finally, the ejecta of core-collapse supernovae (CCSNe). In our Galaxy, most of the dust is produced by low-mass stars ascending the AGB. However, their long evolutionary main-sequence lifetime (a few Gyr) excludes them from being possible dust contributors at high redshift. Conversely, very massive stars evolve much more rapidly (timescales ~ 1 Myr), and can be possible dust makers in the early universe. As to the first generation of stars, hereafter Pop III stars, they are expected to be very massive (Omukai & Nishi 1998; Abel et al. 2002; Bromm et al. 2002). Indeed in the absence of metals, the cooling in primordial clouds is only provided by molecular hydrogen and thus precludes efficient gas fractionation. These Pop III stars first need to synthesize heavy elements by thermonuclear reactions in their cores and reach their explosive ends to possibly condense dust in their massive supernova ejecta. Therefore, pair-instability supernovae (PISNe)

are perhaps the first dust contributors to the pristine, young universe.

The buildup of a molecular phase is a prerequisite to dust nucleation and condensation. Indeed, it provides the molecular precursors from which dust forms and its composition depends on the initial elemental composition of the gas and the physical processes pertaining to it. Furthermore, molecules produced in the early universe can have an important effect on the cooling of the interstellar medium. Molecules have been detected in low-redshift CCSNe as early as 100 days post-explosion. Specifically, the IR rovibrational transitions of CO and SiO were detected in SN1987A (Catchpole et al. 1988; Spyromilio et al. 1988; Meikle et al. 1989; Roche et al. 1991), CO first overtone bands were observed in the Type II SNe SN1995ad (Spyromilio & Leibundgut 1996), SN1998s (Gerardy et al. 2000), and SN2002hh (Pozzo et al. 2006), while SiO detection was reported by Kotak et al. (2006, 2009) in SN2005af and SN2004et, respectively. More recently, detection of CO with the *Spitzer* satellite in Cas A, a 300 year old supernova remnant, is reported by Rho et al. (2009). It is therefore reasonable to expect molecules to form in the ejecta of massive Pop III star SNe.

Existing models for CO and SiO formation in SN1987A ejecta only considered a limited number of chemical processes applicable to low-temperature gases and assumed that steady state held for chemistry in calculating the evolution of molecular masses (Petuchowski et al. 1989; Lepp et al. 1990; Liu et al. 1992; Liu & Dalgarno 1994, 1995, 1996; Clayton et al. 1999, 2001; Gearhart et al. 1999). Models for the formation of dust in SN1987A and PISNe used a classical nucleation theory

approach to describe the growth of solids in the ejecta, ignoring the nucleation stage of dust, in which gas-phase species and dust molecular precursors are formed (Kozasa et al. 1989; Todini & Ferrara 2001; Nozawa et al. 2003 (hereafter NK03); Schneider et al. 2004 (hereafter SFS04)). Since the amount of carbon and oxygen locked up in CO is a major factor in determining the dust composition, Todini & Ferrara (2001) and SFS04 do consider the formation of CO in fully microscopically mixed ejecta. However, their treatment is extremely oversimplified as their CO chemistry includes only two chemical processes and is assumed once again at steady state. In a first attempt to model molecular formation with a chemical kinetic approach in fully microscopically mixed Pop III SN ejecta, Cherchneff & Lilly (2008, hereafter CL08) show that the chemistry does not reach a steady state over the timespan studied. Furthermore, they identified other chemical processes than those considered by SFS04 that are of paramount importance to the formation of CO and other molecular species in the ejecta.

In this paper, we study the formation and evolution of molecules, including gas-phase dust precursors, in the ejecta of Pop III SNe. We define a large set of chemical reactions relevant to the dense and hot SN environment but applicable to other circumstellar media as well. In addition to this extensive reaction network, with new updated rates compared to those used by CL08, we include processes unique to the radioactive environment of SN ejecta: destructive processes induced by Compton electrons created by the downscattering of γ -rays, and by ultraviolet (UV) photons emitted by collisionally excited atoms and ions. We consider fully microscopically mixed and unmixed ejecta for different progenitor masses. In addition, the presence of hydrogen and helium can dramatically affect the chemistry of the ejecta. We therefore examine the impact of the inward diffusion of hydrogen and its effect on the molecular yield of the SNe.

The molecular budgets of SN ejecta are determined by their physical conditions and composition. In Section 2, we describe the relevant parameters: explosion energy, initial density, the ejecta mass, and composition of the SNe under study. These are used to follow the evolution of ejecta temperature and density as a function of time. The reactions taking place in the different layers of the ejecta depend on the degree of elemental mixing, and the section also describes the prescriptions we used to characterize this process. The different mechanisms pertaining to the ejecta chemistry are described in Section 3. We first give a brief overview of the mathematical formalism, followed by a detailed description of the nonthermal destructive processes that operate in an SN environment. The results of our calculations for mixed and unmixed ejecta of various mass progenitors are presented in Section 4, and in Section 5 we briefly summarize and discuss the different implications of these results. Models for the formation of dust precursors in similar environments will be presented in a forthcoming paper (I. Cherchneff & E. Dwek 2009, in preparation).

2. MODEL INPUT PARAMETERS

2.1. Physical Conditions of the Ejecta

Currently, there are no observational constraints on the Pop III SNe events and the evolution of their explosive ejecta. We therefore base our ejecta models on available theoretical explosion models, in particular those of Heger & Woosley (2002), Umeda & Nomoto (2002, hereafter UN02), and NK03. Using these models, we derive simple analytical expressions for

the gas parameters such as temperature, number density, and velocity, and consider various levels of mixing in the ejecta. Three progenitor masses are studied: two massive progenitors of mass $170 M_{\odot}$ and $270 M_{\odot}$ chosen as surrogates to PISNe, and one low-mass $20 M_{\odot}$ progenitor chosen to describe primordial CCSNe.

The gas temperature T in the post-explosion ejecta is determined mainly by the explosion energy which is released as kinetic energy into the gas. NK03 present various models of ejecta for CCSNe, PISNe, and hypernovae. Each model is characterized by an explosion energy, a mass cut marking the division between the matter which remains in the core and that which is ejected and the ^{56}Ni mass produced in the explosion above the mass cut. By solving the radiative transfer equation taking into account the energy deposition by radioactive elements, NK03 derive temperature profiles for each of their massive progenitor ejecta. For our PISNe models, we chose the NK03 temperature profile of the oxygen-rich region for their $170 M_{\odot}$ PISN unmixed case to describe our $170 M_{\odot}$ ejecta temperature variation with time. The temperature characterizing the helium core of PISNe modeled by Fryer et al. (2001) stays almost constant over the core extent. We then assume a constant temperature in the inner He core region so that temperature is independent of the mass coordinate M_r and simply fit the profile by the following power law of degree five

$$T(t) = T_0 \times (A - Bx + Cx^2 - Dx^3 + Ex^4 - Fx^5), \quad (1)$$

where $T_0 = 21,000$ K is the gas temperature at some fiducial time $t_0 = 100$ days, $x = t/t_0$, and the fitting coefficients A , B , C , D , E , and F are equal to 1.699 , 8.568×10^{-1} , 1.761×10^{-1} , 1.762×10^{-2} , 8.229×10^{-4} , and 1.331×10^{-5} , respectively. Our $270 M_{\odot}$ temperature profile is assumed to follow the same variation with time as given in Equation (1). To account for the greater kinetic energy imparted by the explosion of a $270 M_{\odot}$ progenitor, we multiply T_0 by a multiplying factor of 1.5. This value corresponds to the ratio of the central temperatures for the $170 M_{\odot}$ and $270 M_{\odot}$ progenitor models of Heger & Woosley (2002).

For our CCSNe model, we assume that the gas temperature follows the variation of the C20 unmixed model of NK03. Assuming the ejecta follows quasi-adiabatic expansion, the temperature evolution with time is given by

$$T(t) = T_0 \times \left(\frac{t}{t_0}\right)^{3(1-\gamma)}, \quad (2)$$

where γ is an ‘‘adiabatic’’ index. Using Equation (2) to fit the NK03 C20 temperature profile gives a γ value of 1.593.

The ejecta expansion becomes homologous a few hours after explosion so that the gas density varies with time according to

$$\rho(M_r, t) = \rho(M_r, t_0) \times \left(\frac{t}{t_0}\right)^{-3}, \quad (3)$$

where M_r is the mass coordinate. As for temperature, and according to the PISN models of Fryer et al. (2001), we assume a constant gas density over the helium core so that no dependence with the mass coordinate is considered. The gas density profile chosen in the present study is that of NK03 for their $20 M_{\odot}$ and $170 M_{\odot}$ progenitors, assuming $\rho(600 \text{ days})$ equals to $3 \times 10^{-14} \text{ g cm}^{-3}$ for all progenitor masses we study.

The gas number density $n(t)$ for each model is given by

$$n(M_r, t) = \rho(M_r, t) / \mu_{\text{gas}}(t), \quad (4)$$

Table 1
Primordial Supernova Parameters Used in this Study (adapted from UN02, Heger & Woosley 2002, and NK03)

Parameter	20 M_{\odot}	170 M_{\odot}	270 M_{\odot}
$E_{\text{explosion}}$ (erg)	1×10^{51}	2×10^{52}	8×10^{52}
He core mass (M_{\odot})	5.8	82.3	129
$M(^{56}\text{Co})$ (M_{\odot})	0.07	3.6	9.8
v (km s $^{-1}$)	2242	3439	5458
T_0 (K)	18,000	21,000	31,500
τ_0	23.80	146.07	90.89

where $\mu_{\text{gas}}(t)$ is the mean molecular weight of the gas, which varies with time as the chemical composition of the ejecta changes due to molecule formation.

For the sake of simplicity, we define a constant ejecta velocity v determined by the explosion energy of the progenitor through its conversion to kinetic energy and given by

$$v = \sqrt{\frac{2 \times E_0}{M_{\text{ej}}}}, \quad (5)$$

where E_0 is the explosion energy and M_{ej} is the mass ejected above mass cut during explosion. Explosion energies for the present models are listed in Table 1. The respective ejected masses are assumed to be equal to the progenitor masses as Pop III stars do not experience mass loss during their evolution due to the lack of dredged-up metals in their photospheric composition and the consequent wind acceleration through metallic lines. The velocity is assumed to be constant over the mass zones in the ejecta.

We are interested in studying the chemistry from time $t_0 = 100$ days to $t = 1000$ days. The initial time range is justified by the appearance of CO, SiO, and dust as early as 110, 160, and 450 days, respectively, in the ejecta of SN1987A (Catchpole et al. 1988; Danziger et al. 1991; Wooden et al. 1993). Our PISN ejecta are hotter than that of SN1987A but similar temperature regimes are encountered at times $t \geq 300$ days. The final time is determined by the time when the gas density and temperature in the ejecta are too low to foster efficient gas-phase molecular formation. The ejecta parameters are summarized in Table 1, whereas the variation of the gas density and temperature with time t is illustrated in Figure 1 for the various progenitor masses considered.

2.2. Mixing in the Ejecta

Mixing is likely to occur during explosion for the instability of the nickel bubble resulting in the development of Rayleigh–Taylor instabilities (Woosley 1988; Arnett 1988; Herant & Benz 1991; Müller et al. 1991; Kifonidis et al. 2003) and instabilities developing in the post-shocked regions of the propagating blast wave (Chevalier 1976; Bandiera 1984; Benz & Thielemann 1990). Evidence for strong ^{56}Ni mixing in the shell of SN1987A is found through observation of hard X-rays stemming from $^{56}\text{Ni}/^{56}\text{Co}$ decay and γ -rays downscattering as early as 140 days after explosion (Itoh et al. 1987; Pinto & Woosley 1988; Sunyaev et al. 1990). Another direct evidence for heavy element mixing comes from the extraction and study of isotopically anomalous inclusions in meteorites. The presence of type X silicon carbide (SiC) grains and silicon nitride (Si_3N_4) inclusions bearing the ^{44}Ti supernova signature in meteorites suggests deep and inhomogeneous mixing between the various heavy element mass shells (Zinner 2006). As to light elements, hydrogen

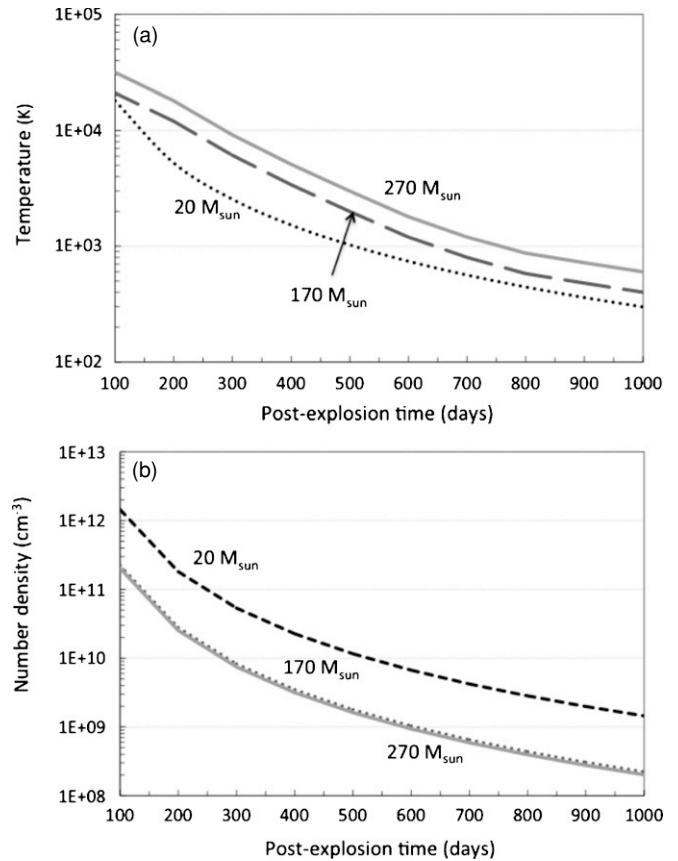


Figure 1. Evolution of the gas parameters as a function of time for the different SN ejecta (taken from Nozawa et al. 2003) and assumed to be independent of mass zone within the He core. (a) Temperature where the 270 M_{\odot} profile has been rescaled by a factor of 1.5 compared to that of the 170 M_{\odot} ejecta to account for the larger explosion energy. (b) Number density.

deep mixing down to the inner mass zones is invoked to explain the plateau shape of SN1987A light curve at times greater than 80 days (Woosley 1988; Arnett & Fu 1989; Shigeyama & Nomoto 1990). However, H mixing is likely to occur at a macroscopic level with the formation of H-rich bubbles in the unstable layer located between the He–CO and the H–He interfaces as early as a few hours after explosion (Fryxell et al. 1991; Herant & Benz 1991; Müller et al. 1991; Burrows & van Riper 1995; Kifonidis et al. 2003). Some hydrogen diffusion may also occur at the base of the hydrogen envelope where helium and heavy element-rich fingers are simultaneously present (Müller et al. 1991; Kifonidis et al. 2003). To circumvent the problem of the complexity of mixing, NK03 considered explosive models with and without mixing, which result in two extreme cases for their ejecta: a fully mixed gas and a stratified ejecta in which each layer reflects the prior nucleosynthesis stages of the progenitor, except for the innermost layer which is the result of explosive nucleosynthesis. We follow the same strategy in the present paper: for the two very massive progenitors, 170 M_{\odot} and 270 M_{\odot} and the core-collapse SN progenitor, 20 M_{\odot} , we consider fully mixed ejecta, while stratified ejecta are studied for the 170 M_{\odot} and 20 M_{\odot} progenitors.

2.3. Initial Ejecta Composition

The initial chemical compositions for the primordial supernova ejecta models are taken from fully mixed and unmixed explosion models. For fully mixed ejecta, mass yields are from

Table 2
Initial (Post-explosive) Chemical Composition in Units of M_{\odot} for Fully Mixed Primordial SN Ejecta Without Hydrogen Mixing

M_{prog}	$\mu_0(\text{gas})$	He	O	Si	S	Mg	Fe	C	Al	Ne	Ar	N
20 M_{\odot}	5.63	3.59	1.55	9.82 (−2)	4.12 (−2)	7.07 (−2)	7 (−2)	0.26	4.79 (−4)	0.12	6.9 (−3)	2.69 (−4)
170 M_{\odot}	18.11	1.96	44.23	16.16	8.66	1.94	3.63	2.30	2.0 (−2)	1.19	1.42	1.0 (−2)
270 M_{\odot}	19.31	5.5	44.31	26.95	15.78	4.78	16.14	1.89	8.62 (−2)	4.70	2.60	1.26 (−2)

Note. The initial mean molecular weight $\mu_0(\text{gas})$ is given in g mole^{-1} .

Table 3
Initial (post-explosive) Chemical Composition in Units of M_{\odot} for Unmixed Primordial SN Ejecta

Zone	$\mu_0(\text{gas})$	C/O	He	O	Si	S	Mg	Fe	C	Al	Cr	Co	Ni
Unmixed 20 M_{\odot}													
Zone 1 (2.4–3 M_{\odot})	30.21	0.013	0	6 (−4)	0.39	0.138	6 (−6)	0.048	6 (−6)	1.2 (−7)	3 (−3)	4 (−4)	2 (−4)
Zone 2 (3–3.6 M_{\odot})	16.87	0.0013	0	0.52	0.0358	0.0072	0.0363	0	4.98 (−4)	4.2 (−5)	0	0	0
Zone 3 (3.6–4.95 M_{\odot})	15.03	0.33	0	1.08	2.7 (−5)	6.75 (−7)	4.725 (−3)	0	0.266	4.05 (−6)	0	0	0
Zone 4 (4.95–5.85 M_{\odot})	4.05	29.47	0.884	6.84 (−4)	9.0 (−9)	0	2.25 (−5)	0	1.512 (−2)	0	0	0	0
Unmixed 170 M_{\odot}													
Zone 1 (0–20 M_{\odot})	29.13	0.066	0	3.5 (−5)	13.2	4.0	5.3 (−5)	0.35	1.8 (−6)	1.8 (−10)	3.5 (−3)	1.2 (−3)	3.5 (−3)
Zone 2 (20–40 M_{\odot})	17.29	2.9×10^{-5}	0	16.5	2.76	0.4	0.32	0	3.6 (−4)	5 (−4)	0	0	0
Zone 3 (40–55 M_{\odot})	16.76	0.03	0	13.1	0.615	3 (−2)	1.22	0	3 (−2)	1.5 (−2)	0	0	0
Zone 4 (55–78 M_{\odot})	15.17	0.29	0	18.6	1.84 (−3)	1.38 (−6)	0.299	0	4.07	4.6 (−4)	0	0	0
Zone 5 (78–82 M_{\odot})	10.46	0.56	0.596	2.4	4 (−6)	2.4 (−7)	3.6 (−3)	0	1.0	4 (−8)	0	0	0

Note. The initial mean molecular weight $\mu_0(\text{gas})$ is given (in g mol^{-1}) as well as the C/O ratio of each zone.

UN02 for all progenitor masses. The unmixed ejecta compositions for the 170 M_{\odot} progenitor and the 20 M_{\odot} progenitor are those of NK03. We subdivide their helium cores in zones of distinct chemical composition. For the 170 M_{\odot} progenitor, we consider five distinct zones: (1) is Si/S/Fe-rich from 0 to 20 M_{\odot} ; (2) is O/Si/S-rich from 20 to 40 M_{\odot} ; (3) is O/Mg/Si-rich from 40 to 55 M_{\odot} , (4) is O/C/Mg-rich from 55 to 78 M_{\odot} , and finally (5) is O/C/He-rich from 78 to 82 M_{\odot} . For the 20 M_{\odot} progenitor, the zoning comprises four zones as follows: (1) is Si/S/Fe-rich and extends from 2.4 to 3 M_{\odot} ; (2) is O/Si/S-rich from 3 to 3.6 M_{\odot} ; (3) is O/C/Mg-rich from 3.6 to 4.95 M_{\odot} ; and finally (4) is He/C/O-rich from 4.95 to 5.85 M_{\odot} . For the sake of simplicity, we ignore the variations of the elemental abundances with mass coordinates and take them to be constant within each zone.

We use these elemental mass yields to calculate the total number of elemental species, the gas initial molecular weight $\mu_{\text{gas}}(t_0)$, and gas number density $n(M_r, t_0)$. We then derive the number density at 100 days post-explosion for each element, and use these data as initial conditions when solving our set of nonlinear, coupled, differential equations (see Section 3). These data along with the resulting initial gas mean molecular weight are tabulated in Table 2 for fully mixed ejecta, while Table 3 summarizes the post-explosion chemical composition as a function of zoning for our unmixed ejecta models. We then explore the effect of hydrogen mixing by diffusion from the progenitor envelope for the 170 M_{\odot} fully mixed ejecta. In doing so, we set the H content as a free parameter and assume that H can microscopically mix within the heavy element-rich He core. Values of H mixing ranges from 0% to 10% of the total hydrogen envelope mass given by UN02.

3. EJECTA CHEMISTRY

A chemical kinetic description of the ejecta is based on a gas initial chemical composition and a set of chemical reactions describing the chemical processes at play and applied to the ejecta physical conditions. For the high gas temperatures and densities characterizing our modeled ejecta, they include

1. Termolecular reactions efficient in high-density media and where formation of molecules occurs through collision with the ambient gas which carries away the excess energy of the reaction. We also consider their reverse processes which are thermal fragmentation through collisions with the ambient gas at high temperatures.
2. Bimolecular processes, predominantly neutral–neutral (hereafter NN) reactions. The reactions with activation energy barriers require high temperatures to overcome the energy barrier, whereas reactions without activation energy can proceed at lower temperatures.
3. Ion–molecule reactions (formation/destruction reactions and charge exchange processes), which have no energy barrier and can therefore contribute at low gas temperatures.
4. Temperature-independent radiative association reactions (hereafter RA) in which the formation of a species occurs through the emission of a photon which carries off the excess energy released in the formation of the adduct.

Because of the unique nature of SN ejecta, being powered by the decay of radioactive elements and its high temperatures, we also consider the effects of various nonthermal processes including the destruction of molecules by the cascade of energetic electrons and UV photons that are generated by the downscattering of γ -rays in the ejecta. These nonthermal processes will be discussed in more details in the following section.

The temporal variation of the number density of a molecular specie i located in a given mass zone M_r is described by the following rate equation:

$$\frac{\partial n_i(M_r, t)}{\partial t} = P_i - L_i = \sum_j k_{ji} n_j n_i - \sum_k k_{ik} n_i n_k, \quad (6)$$

where P_i are the production (\equiv formation) processes and L_i are the loss (\equiv destruction) processes for species i , and k_{ji} and k_{ik} are the temperature-dependent rates for reactions between species i – j and i – k , respectively. The reaction rates k_{ji} and k_{ik} are written

Table 4
Species Included in the Ejecta Chemical Models

Species Type	Species										
Atoms	H	He	O	C	Si	S	Mg	Fe	Al		
Diatomic species	H ₂	OH	O ₂	CO	SiO	SO	NO	MgO	FeO	AlO	C ₂
	CS	CN	SiH	SiC	Si ₂	SiS	SiN	SH	N ₂	NH	MgS
	Fe ₂										
Tri-atomic species	H ₂ O	H ₂ S	HCN	CH ₂	C ₂ H	HCO	C ₃	CO ₂	OCS	OCN	SiC ₂
	Si ₃	SiO ₂	SO ₂	NO ₂	Fe ₃						
Four-atom species	Si ₂ O ₂	Mg ₂ O ₂	Mg ₂ S ₂	Fe ₂ O ₂	Fe ₂ S ₂	H ₂ CC	Fe ₄	Si ₄	C ₃ H	CH ₃	
≥Five-atom species	Si ₃ O ₃	Si ₂ O ₄	Si ₃ O ₆	C ₃ H ₃	C ₄ H ₄	C ₆ H ₅	C ₆ H ₆				
Ions	H ⁺	H ⁻	He ⁺	O ⁺	Si ⁺	S ⁺	Mg ⁺	Fe ⁺	Al ⁺	H ₂ ⁺	H ₃ ⁺
	HeH ⁺	C ₂ ⁺	CO ⁺	SiO ⁺	SO ⁺	H ₂ O ⁺	HCO ⁺				

under the form of Arrhenius expressions, such as

$$k_{ij}(T) = A_{ij} \times \left(\frac{T}{300}\right)^{\nu} \times \exp(-E_{ij}/T), \quad (7)$$

where T is the temperature given by Equations (1) and (2), A_{ij} the Arrhenius coefficient in s^{-1} molecule⁻¹, cm^3 or $cm^6 s^{-1}$ molecule⁻¹ for a unimolecular, bimolecular, or termolecular processes, respectively, ν reflects the temperature dependence of the reaction, and E_{ij} is the activation energy barrier in K^{-1} . The ensemble of equations as in Equation (6) represents a set of N nonlinear, coupled, ordinary differential equations to solve, where N is the number of species (atoms, ions, molecules, and electrons) included in the chemical description of the ejecta. In total, the system comprises up to 83 species listed in Table 4 and between 400 and 500 reactions, depending on the ejecta region under study. The full chemical scheme is listed in Table 5. Reaction rates have either been measured under laboratory conditions or theoretically calculated using transition state theory. When not documented, the rates are estimated using “educated” guesses. The NIST chemical kinetics database is used as primary source for NN processes, completed by the UDFAO6 database (Woodall et al. 2007) when necessary. The numbering of some reactions specified in the text refers to that of Table 5. For dust precursor formation, processes and reaction rates stem from combustion chemistry studies, environmental and material sciences, and full details are given in I. Cherchneff & E. Dwek (2009, in preparation).

3.1. Nonthermal Processes

3.1.1. Destruction by Compton Electrons

A supernova explosion produces ⁵⁶Ni which rapidly decays to ⁵⁶Co with a half-life of 6 days, which in turn decays to ⁵⁶Fe with a half-life of ~77 days. The decay of ⁵⁶Co deposits 3.57 MeV in the form of γ -rays in the ejecta, which powers the SN light curve (Woosley et al. 1989). Compton scattering degrades the γ -rays, which have an average energy of 1.24 MeV, to hard X-rays which through a cascade of inverse Compton, ionization, and recombination processes degrade further into UV photons. The fast Compton electrons thermalize by heating, exciting, and ionizing the ejecta, adding to the reservoir of UV photons. In SN1987A, the light curve between days 100 and 1000 could be reproduced if 0.075 M_{\odot} of ⁵⁶Co was ejected in the explosion.

The fast Compton electrons and UV radiation can have a significant effect on the chemistry of the ejecta. Compton electrons were proposed in several studies to be one of the

dominant destruction routes to molecules in SN ejecta (Liu & Dalgarno 1994, 1995, 1996). Clayton et al. (1999, 2001) furthermore suggested that atomic carbon and carbon dust could be produced in oxygen-rich part of the ejecta by CO dissociation due to collision with Compton electrons. We therefore pay special attention to deriving destruction rates for similar radioactivity-induced processes in the ejecta of our primordial SNe. In addition, we will also explore the role of UV photons on the chemistry of the ejecta.

Not all the radioactive decay is deposited in the ejecta. The early emergence of γ -rays and X-rays a few hundred days after the explosion of SN1987A provides strong evidence that the ejecta in macroscopically mixed and presumably clumpy (McCray 1993). However, the fraction of this escaping energy is small, and throughout this paper we will assume that all the radioactive energy is deposited uniformly in the ejecta. The rate of energy deposition by thermalized ⁵⁶Co γ -rays in the ejecta of SN1987A is given by (Woosley et al. 1989)

$$L_{\gamma} = 9.54 \times 10^{41} \times \exp(-t/\tau_{56}) \times (1 - \exp[-\tau_0(t/t_0)^{-2}]), \quad (8)$$

where L_{γ} is given in $erg s^{-1}$, $\tau_{56} = 111.26$ d is the e-folding time of ⁵⁶Co decay, and τ_0 is the effective γ -ray optical depth of the ejecta at some fiducial time t_0 . L_{γ} scales linearly with the mass of ⁵⁶Co in the ejecta. Therefore, the destruction rate by Compton electrons for species i in s^{-1} per particle, k_C , can be written in terms of M_{56} (1987A), the mass of ⁵⁶Co produced in SN1987A, as (Liu & Dalgarno 1995; CL08)

$$k_C(i) = \frac{5.95 \times 10^{53}}{W_i \times N_i} \left[\frac{M_{56}}{M_{56}(\text{SN1987A})} \right] \times \exp(-t/\tau_{56}) \times (1 - \exp[-\tau_0(t/t_0)^{-2}]), \quad (9)$$

where N_i is the total number of particles of species i , M_{56} is the mass of ⁵⁶Co in the ejecta of the SN being studied, and W_i is the mean energy (in eV) per ion-pair, dissociation or excitation for species i . W_i is defined as the ratio of the energy of the incident electron divided by the number of ionization, dissociation, or excitation produced by collision with the incident electron until it comes to rest (Liu & Dalgarno 1994; Dalgarno et al. 1999).

The effective γ -ray optical depth $\tau(t)$ at time t can be written as

$$\begin{aligned} \tau(t) &\equiv \kappa_{56} \times \phi(t) \\ &= \kappa_{56} \times \rho(t) R(t) = \kappa_{56} \times \left(\frac{3 M_{\text{He}}}{4 \pi R(t)^2} \right), \end{aligned} \quad (10)$$

Table 5
Chemical Processes Considered in the Present Study

No.	Chemical Processes		A	ν	E_a	Reference ^a	
TERMOLÉCULAR							
3B1	H + H + M	→	H ₂ + M	6.84×10^{-33}	-1	0	NIST
3B2	H + C + M	→	CH + M	1.00×10^{-33}	0	0	E
3B3	H + O + M	→	OH + M	4.36×10^{-32}	-1	0	NIST
3B4	H + OH + M	→	H ₂ O + M	2.59×10^{-31}	-2	0	NIST
3B5	H + CN + M	→	HCN + M	8.63×10^{-30}	-2.2	566.5	NIST
3B6	H + CO + M	→	HCO + M	5.29×10^{-34}	0	370.4	NIST
3B7	H + C ₂ + M	→	C ₂ H + M	1.00×10^{-33}	0	0	E
3B8	H + C ₃ + M	→	C ₃ H + M	1.00×10^{-33}	0	0	E
3B9	O + C + M	→	CO + M	2.14×10^{-29}	-3.08	-2114.0	UDFA06
3B10	O + O + M	→	O ₂ + M	9.26×10^{-34}	-1	0	NIST
3B11	O + S + M	→	SO + M	9.26×10^{-34}	-1	0	E as 3B9
3B12	O + N + M	→	NO + M	5.46×10^{-33}	0	155.1	NIST
3B13	O + CO + M	→	CO ₂ + M	1.20×10^{-32}	0	2160.0	NIST
3B14	O + Si + M	→	SiO + M	2.14×10^{-29}	-3.08	-2114.0	E as 3B9
3B15	C + C + M	→	C ₂ + M	1.00×10^{-33}	0	0	E
3B16	C + C ₂ + M	→	C ₃ + M	1.00×10^{-33}	0	0	E
3B17	C + S + M	→	CS + M	2.14×10^{-29}	-3.08	-2114.0	E as 3B9
3B18	C + N + M	→	CN + M	9.40×10^{-33}	0	0	NIST
3B19	Si + H + M	→	SiH + M	1.00×10^{-33}	0	0	E
3B20	Si + N + M	→	SiN + M	9.40×10^{-33}	0	0	E as 3B17
3B21	Si + S + M	→	SiS + M	2.14×10^{-29}	-3.08	-2114.0	E as 3B9
3B22	S + S + M	→	S ₂ + M	2.76×10^{-33}	0	0	NIST
3B23	N + N + M	→	N ₂ + M	1.25×10^{-32}	0	0	NIST
3B24	CO + CH + M	→	HC ₂ O + M	2.80×10^{-34}	-0.4	0	NIST
3B25	H + CO + H	→	O + CH ₂	1.00×10^{-33}	0	0	E
3B26	H + CO ₂ + H	→	O ₂ + CH ₂	1.00×10^{-33}	0	0	E
3B27	H + C ₂ H ₂ + H	→	CH ₂ + CH ₂	1.00×10^{-36}	0	0	E
3B28	CO + OH + H	→	O ₂ + CH ₂	1.00×10^{-33}	0	0	E
THERMAL FRAGMENTATION							
TF1	H ₂ + M	→	H + H + M	2.54×10^{-8}	-0.1	52555.6	NIST
TF2	CH + M	→	C + H + M	3.16×10^{-10}	0	33700.0	NIST
TF3	OH + M	→	O + H + M	4.00×10^{-9}	-0.1	50000.0	NIST
TF4	SiH + M	→	Si + H + M	3.16×10^{-10}	0	33700.0	E as TF2
TF5	H ₂ O + M	→	OH + H + M	5.80×10^{-9}	0	52920.0	NIST
TF6	HCN + M	→	H + CN + M	2.08×10^{-8}	0	54630.0	NIST
TF7	CH ₂ + M	→	CH + H + M	6.64×10^{-9}	0	41852.0	NIST
TF8	CH ₂ + M	→	H ₂ + C + M	2.66×10^{-10}	0	32230.0	NIST
TF9	C ₂ H + M	→	C ₂ + H + M	3.75×10^{-10}	0	50040.0	NIST
TF10	C ₃ H + M	→	C ₃ + H + M	1.00×10^{-10}	0	48600.0	E
TF11	HC ₂ O + M	→	CO + CH + M	1.08×10^{-8}	0	29585.0	NIST
TF12	O ₂ + M	→	O + O + M	5.17×10^{-10}	0	58410.0	NIST
TF13	CO + M	→	C + O + M	4.40×10^{-10}	0	98600.0	Appleton et al. 1970
TF14	SO + M	→	S + O + M	6.61×10^{-10}	0	53885.0	NIST
TF15	SiO + M	→	Si + O + M	4.40×10^{-10}	0	98600.0	E as TF13
TF16	NO + M	→	N + O + M	4.10×10^{-9}	0	75380.0	NIST
TF17	CO ₂ + M	→	CO + O + M	8.02×10^{-11}	0	26900.0	NIST
TF18	C ₂ + M	→	C + C + M	3.02×10^{-9}	0	63980.7	NIST
TF19	CS + M	→	C + S + M	4.40×10^{-10}	0	98600.0	E as TF13
TF20	CN + M	→	C + N + M	3.32×10^{-10}	0	74989.0	NIST
TF21	SiS + M	→	Si + S + M	4.40×10^{-10}	0	98600.0	E as TF13
TF22	SiN + M	→	Si + N + M	3.32×10^{-10}	0	74989.0	E as TF20
TF23	S ₂ + M	→	S + S + M	7.95×10^{-11}	0	38749.0	NIST
TF24	N ₂ + M	→	N + N + M	2.52×10^{-7}	-1.6	57005.4	NIST
NEUTRAL-NEUTRAL							
NN1	H + OH	→	H ₂ + O	6.86×10^{-14}	2.8	1949.5	NIST
NN2	H + H ₂ O	→	OH + H ₂	6.82×10^{-12}	1.6	9720	NIST
NN3	H + O ₂	→	OH + O	6.73×10^{-10}	-0.6	8151.0	NIST
NN4	H + CH	→	C + H ₂	1.31×10^{-10}	-1.6	80.0	NIST
NN5	H + C ₂	→	C + CH	4.67×10^{-10}	0.5	30450.0	UDFA06
NN6	H + CH ₂	→	CH + H ₂	1.00×10^{-11}	0	-899.6	NIST
NN7	H + C ₂ H	→	C ₂ + H ₂	5.99×10^{-11}	0	11800.0	NIST
NN8	H + C ₂ H ₂	→	C ₂ H + H ₂	1×10^{-10}	0	14000.0	NIST
NN9	H + HC ₂ O	→	O + C ₂ H ₂	2.51×10^{-10}	0	0	NIST
NN10	H + HC ₂ O	→	CO + CH ₂	4.98×10^{-11}	0	0	NIST

Table 5
(Continued)

No.	Chemical Processes		A	ν	E_a	Reference ^a	
NN11	H + HCN	→	CN+ H ₂	6.19×10^{-10}	0	12499.0	NIST
NN12	H + CO	→	C+OH	1.1×10^{-10}	0.5	77700.0	UDFA06
NN13	H + CO	→	CO+H	1.0×10^{-16}	0	0	E
NN14	H + CO ₂	→	CO+OH	2.51×10^{-10}	0	13349.0	NIST
NN15	H + CS	→	CH+S	1.2×10^{-11}	0.6	5880.0	UDFA06
NN16	H + SiH	→	Si + H ₂	2.00×10^{-11}	0	0	Willacy & Cherchneff 1998
NN17	H + SiO	→	SiH + O	1.00×10^{-16}	0	0	E as NN13
NN18	H + SiO	→	Si + OH ₂	1.00×10^{-16}	0	0	NN13
NN19	H + SiS	→	SiH+ S	1.00×10^{-16}	0	0	NN13
NN20	H + SO	→	OH+ S	5.90×10^{-10}	-0.3	11100	UDFA06
NN21	H + SO	→	OH+ S	5.90×10^{-10}	-0.3	11100	UDFA06
NN22	H + NO	→	OH+ N	2.82×10^{-10}	0	24560.0	NIST
NN23	O + H ₂	→	OH+H	3.39×10^{-13}	2.7	3159.3	NIST
NN24	O + OH	→	O ₂ + H	4.55×10^{-12}	0.4	-371.6	NIST
NN25	O + H ₂ O	→	OH+ OH	1.85×10^{-11}	1	8750	NIST
NN26	O + CH	→	OH+ C	2.52×10^{-11}	0	2381.0	NIST
NN27	O+ CH	→	CO+ H	6.59×10^{-11}	0	0	NIST
NN28	O+ CH ₂	→	CO+ H ₂	1.33×10^{-11}	0	0	RH01
NN29	O+ CH ₂	→	CO+ H+H	1.33×10^{-10}	0	0	NIST
NN30	O + C ₂ H	→	CO+ CH	1.69×10^{-11}	0	0	NIST
NN31	O+ C ₂ H ₂	→	CO+ CH ₂	2.66×10^{-10}	0	1980.1	NIST
NN32	O+ C ₂ H ₂	→	HC ₂ O+ H ₂	1.19×10^{-12}	2.0	956.1	NIST
NN33	O+ HC ₂ O	→	C ₂ H+ O ₂	1.66×10^{-10}	0	0	NIST
NN34	O+ HC ₂ O	→	CO ₂ H+ CH	1.99×10^{-12}	0	0	NIST
NN35	O + HCN	→	OH+ CN	1.43×10^{-12}	1.5	3799.1	NIST
NN36	O + SiH	→	SiO+ H	1.00×10^{-10}	0	0	UDFA06
NN37	O + CO	→	O ₂ + C	1.00×10^{-16}	0	0	E as NN13
NN38	O + CO ₂	→	CO+ O ₂	2.81×10^{-11}	0	24458.0	NIST
NN39	O + C ₂	→	CO+ C	5.99×10^{-10}	0	0	NIST
NN40	O + CS	→	CO+ S	5.00×10^{-11}	0	0	NIST
NN41	O + CS	→	SO+ C	4.68×10^{-11}	0.5	28940.0	UDFA06
NN42	O + CN	→	CO+ N	1.45×10^{-10}	-0.18	0	NIST
NN43	O + SiO	→	O ₂ + Si	1.00×10^{-16}	0	0	E as NN13
NN44	O + SiN	→	SiO+ N	6.64×10^{-11}	0	0	NIST
NN45	O + SiN	→	NO+ Si	5.00×10^{-11}	0	0	UDFA06
NN46	O + SO	→	O ₂ + S	2.13×10^{-13}	1.5	2536.4	NIST
NN47	O + S ₂ S	→	SO+ S	1.70×10^{-11}	0	0	UDFA06
NN48	O + NO	→	O ₂ + N	2.74×10^{-11}	0	21286.0	NIST
NN49	O + N ₂	→	NO+ N	3.01×10^{-10}	1.0	38244.0	NIST
NN50	O + SiN	→	SiO+ N	6.64×10^{-11}	0	0	NIST
NN51	C + H ₂	→	CH+ H	6.64×10^{-10}	0	11699.2	NIST
NN52	C + OH	→	CO+ H	1.10×10^{-11}	0	0	UDFA06
NN53	C + OH	→	CH+ O	2.25×10^{-11}	0.5	14800.0	UDFA06
NN54	C + H ₂ O	→	CH+ OH	1.20×10^{-12}	0	19776.0	NIST
NN55	C + CH ₂	→	CH+ CH	2.69×10^{-12}	0.5	0	NIST
NN56	C + O ₂	→	CO+ O	2.46×10^{-12}	1.5	-613.0	UDFA06
NN57	C + CO	→	C ₂ + O	5.43×10^{-7}	-1.5	57200.0	Hanson 1973
NN58	C + CO ₂	→	CO+ CO	1.10×10^{-15}	0	0	NIST
NN59	C + SiO	→	CO+ Si	1.00×10^{-16}	0	0	E as NN13
NN60	C + SO	→	CO+ S	3.50×10^{-11}	0	0	UDFA06
NN61	C + SO	→	CS+ O	3.50×10^{-11}	0	0	UDFA06
NN62	C + S ₂	→	CS+ S	7.11×10^{-11}	0	0	UDFA06
NN63	C + S ₂	→	CS+ S	7.11×10^{-11}	0	0	UDFA06
NN64	C + NO	→	CO+ N	3.49×10^{-11}	0	0	NIST
NN65	C + NO	→	CN+ O	5.57×10^{-11}	-0.3	0	NIST
NN66	C + N ₂	→	CN+ N	8.69×10^{-11}	0	22600.0	NIST
NN67	Si + H ₂	→	SiH+ H	6.64×10^{-10}	0	11699.0	E as NN51
NN68	Si + OH	→	SiO+ H	3.32×10^{-10}	0	0	NIST
NN69	Si + O ₂	→	SiO+ O	1.72×10^{-10}	-0.5	16.8	NIST
NN70	Si + CO	→	SiO+ C	1.30×10^{-9}	0	34516.0	NIST
NN71	Si + CO ₂	→	SiO+ CO	9.96×10^{-10}	0	9419.1	NIST
NN72	Si + S ₂	→	SiS+ S	7.00×10^{-11}	0	0	E as NN62
NN73	Si + NO	→	SiO+ N	5.31×10^{-11}	0	1779.9	NIST
NN74	Si + O ₂	→	SiO+ O	1.72×10^{-10}	-0.5	16.8	NIST
NN75	S + OH	→	SO+ H	6.59×10^{-11}	0	0	NIST
NN76	S + O ₂	→	SO+ O	1.39×10^{-12}	0.5	15.0	NIST
NN77	S + CH	→	CS+ H	6.59×10^{-11}	0	0	E as NN27

Table 5
(Continued)

No.	Chemical Processes		A	ν	E_a	Reference ^a	
NN78	S + CO	→	SO+ C	1.00×10^{-16}	0	0	E as NN13
NN79	S + CO	→	CS+ O	1.00×10^{-16}	0	0	E as NN13
NN80	S + CS	→	S ₂ + C	1.73×10^{-11}	0.5	11500	E as NN83
NN81	S + CN	→	CS+ N	1.45×10^{-10}	-0.2	0	E as NN42
NN82	S + SiS	→	S ₂ + Si	4.68×10^{-11}	0.5	22	E as NN44
NN83	S + SO	→	S ₂ + O	1.73×10^{-11}	0.5	11500.0	UDFA06
NN84	S + NO	→	SO+ N	1.75×10^{-10}	0	20200.0	UDFA06
NN85	N + OH	→	NO+ H	4.00×10^{-11}	0	0	NIST
NN86	N + HCN	→	N ₂ + CH	3.00×10^{-10}	0	0	E as NN91
NN87	N + O ₂	→	NO+ O	3.44×10^{-12}	1.2	4000	NIST
NN88	N + CO	→	NO+ C	3.84×10^{-9}	0	35959.0	NIST
NN89	N + CO	→	CN+ O	3.83×10^{-9}	0	35990.0	NIST
NN90	N + CO ₂	→	NO+ CO	3.20×10^{-13}	0	1710.5	NIST
NN91	N + CN	→	N ₂ + C	3.00×10^{-10}	0	0	NIST
NN92	N + CS	→	CN+ S	3.80×10^{-11}	0.5	1160.0	UDFA06
NN93	N + SiO	→	SiN+ O	3.84×10^{-9}	0	35959.0	E as NN88
NN94	N + SiO	→	NO+ Si	1.00×10^{-16}	0	0	E as NN13
NN94	N + SiS	→	SiN+ S	3.80×10^{-11}	0	1160.0	E as NN92
NN94	N + SO	→	NO+ S	1.73×10^{-11}	0.5	750	UDFA06
NN95	N + NO	→	N ₂ + O	7.11×10^{-11}	0	786.1	NIST
NN96	H ₂ + OH	→	H ₂ O+ H	2.97×10^{-12}	1.2	2370.4	NIST
NN97	H ₂ + CH	→	CH ₂ + H	1.48×10^{-11}	1.8	839.4	NIST
NN98	H ₂ + C ₂ H	→	C ₂ H ₂ + H	8.95×10^{-13}	2.6	129.9	NIST
NN99	H ₂ + CO ₂	→	CH ₂ + O ₂	1.00×10^{-16}	0	0	E as NN13
NN100	H ₂ + CO	→	CH ₂ + O	1.00×10^{-33}	0	0	E
NN101	H ₂ + O ₂	→	OH+ OH	3.16×10^{-10}	0	21890.0	NIST
NN102	H ₂ + C ₂	→	C ₂ H+ H	1.10×10^{-10}	0	4000.0	NIST
NN103	H ₂ + CN	→	HCN+ H	5.65×10^{-13}	2.4	1129.9	NIST
NN104	OH + CH	→	H ₂ O+ C	1.00×10^{-16}	0	0	E as NN13
NN109	OH + C ₂ H ₂	→	HC ₂ O+ H ₂	1.91×10^{-13}	0	-0	NIST
NN105	OH + OH	→	H ₂ + O ₂	1.65×10^{-12}	1.1	6013.2	UDFA06
NN106	OH + OH	→	H ₂ O+ O ₂	1.65×10^{-12}	1.1	50.0	UDFA06
NN107	OH + CO	→	H+ CO ₂	3.75×10^{-14}	1.6	-401.9	NIST
NN108	OH + CO	→	CH+ O ₂	1.00×10^{-16}	0	0	E as NN13
NN110	OH + CN	→	H+ CO ₂	3.75×10^{-14}	1.6	-401.9	NIST
NN111	OH + HCN	→	H ₂ O+CN	2.41×10^{-11}	0	5499.7	NIST
NN112	O ₂ + CH	→	CO+ OH	8.00×10^{-11}	0	0	NIST
NN113	O ₂ + CH ₂	→	H ₂ + CO ₂	1.33×10^{-11}	0	0	RH01
NN114	O ₂ + CH ₂	→	H ₂ O+ CO	2.54×10^{-10}	-3.3	1443.0	RH01
NN115	O ₂ + CH ₂	→	CO ₂ + H+H	1.33×10^{-11}	0	0	RH01
NN116	O ₂ + CH ₂	→	CO+ OH+H	1.33×10^{-11}	0	0	RH01
NN117	O ₂ + C ₂ H	→	HC ₂ O+ O	1.00×10^{-12}	0	0	NIST
NN118	O ₂ + CO	→	CO ₂ + O ₂	4.20×10^{-12}	0	24053.0	NIST
NN119	O ₂ + N ₂	→	NO+ NO	1.00×10^{-16}	0	0	E as NN13
NN120	CH ₂ + CH ₂	→	C ₂ H ₂ +H+H	3.32×10^{-10}	0	5229.8	NIST
NN121	CH ₂ + CH ₂	→	C ₂ H ₂ +H ₂	2.62×10^{-9}	0	6009.6	NIST
NN122	CO + CH	→	C ₂ H+O	1.00×10^{-16}	0	0	E as NN13
NN123	CO + CH ₂	→	C ₂ H ₂ +O	1.00×10^{-16}	0	0	NIST
NN124	CO + SiO	→	CO ₂ +Si	1.00×10^{-16}	0	0	E as NN13
NN125	CO + NO	→	CO ₂ +N	1.00×10^{-16}	0	0	E as NN13
NN126	CN + H ₂ O	→	HCN+ OH	1.25×10^{-11}	0	3719.0	NIST
NN127	NO + NO	→	N ₂ + O ₂	2.51×10^{-11}	0	30653.0	UDFA06

RADIATION ASSOCIATION

RA1	H + H ⁺	→	HeH ⁺ + h ν	5.26×10^{-20}	-0.5	0	UDFA06
RA2	He + H ⁺	→	H ₂ ⁺ + h ν	5.13×10^{-19}	1.8	0	UDFA06
RA3	O + O	→	O ₂ + h ν	1.00×10^{-19}	0	0	Babb & Dalgarno 1995
RA4	O + C	→	CO + h ν	1.58×10^{-17}	0.3	1297.4	Dalgarno et al. 1990
RA5	O + C ⁺	→	CO ⁺ + h ν	3.14×10^{-18}	-0.1	68.0	Dalgarno et al. 1990
RA6	O + Si	→	SiO + h ν	5.52×10^{-18}	0.3	0	Andreazza et al. 1995
RA7	O + Si ⁺	→	SiO ⁺ + h ν	5.50×10^{-18}	0	0	Andreazza et al. 1995
RA8	O + S	→	SO + h ν	1.11×10^{-19}	0.3	1297.9	Andreazza & Marinho 2005
RA9	C + O ⁺	→	CO ⁺ + h ν	3.14×10^{-18}	-0.1	68.0	UDFA06
RA10	C + C	→	C ₂ + h ν	4.36×10^{-18}	0.3	161.3	Singh & Andreazza 2000
RA11	C + C ₂	→	C ₃ + h ν	1.00×10^{-17}	0	0	Clayton et al. 1999
RA12	C + S	→	CS + h ν	4.36×10^{-19}	0.2	0	Andreazza & Marinho 2005
RA13	C + N	→	CN + h ν	7.87×10^{-19}	0	96.0	Singh & Andreazza 2000

Table 5
(Continued)

No.	Chemical Processes		A	ν	E_a	Reference ^a	
RA14	Si + S	→	CS + h ν	1.05×10^{-19}	0.3	66.1	Andreazza & Marinho 2007
RA15	S + S	→	S ₂ + h ν	1.38×10^{-19}	0.3	-78.8	Andreazza & Marinho 2005
ION-MOLECULE							
IM1	H ₂ ⁺ + He	→	HeH ⁺ + H	1.30×10^{-10}	0	0	UDFA06
IM2	H ₂ ⁺ + H ₂	→	H ₃ ⁺ + H	2.08×10^{-9}	0	0	UDFA06
IM3	H ₃ ⁺ + O	→	OH ⁺ + H ₂	8.40×10^{-10}	0	0	UDFA06
IM4	H ₃ ⁺ + Mg	→	Mg ⁺ + H ₂ + H	1.00×10^{-9}	0	0	UDFA06
IM5	H ₃ ⁺ + Fe	→	fe ⁺ + H ₂ + H	4.90×10^{-9}	0	0	UDFA06
IM6	HeH ⁺ + H	→	H ₂ ⁺ + He	9.10×10^{-10}	0	0	UDFA06
IM7	HeH ⁺ + H ₂	→	H ₃ ⁺ + He	1.50×10^{-9}	0	0	UDFA06
IM8	He ⁺ + H ₂	→	He + H ⁺ + H	1.10×10^{-9}	0	0	UDFA06
IM9	He ⁺ + OH	→	O ⁺ + H + He	1.10×10^{-9}	0	0	UDFA06
IM10	He ⁺ + OH	→	O + H ⁺ + He	1.10×10^{-9}	0	0	UDFA06
IM11	He ⁺ + H ₂ O	→	OH + H ⁺ + He	2.04×10^{-10}	0	0	UDFA06
IM12	He ⁺ + O ₂	→	O ⁺ + O + He	1.10×10^{-9}	0	0	UDFA06
IM13	He ⁺ + CO	→	C ⁺ + O + He	1.40×10^{-9}	-0.5	0	UDFA06
IM14	He ⁺ + CO ₂	→	CO ⁺ + O + He	8.70×10^{-10}	0	0	UDFA06
IM15	He ⁺ + C ₂	→	C ⁺ + C + He	1.60×10^{-9}	0	0	UDFA06
IM16	He ⁺ + CH ₂	→	C ⁺ + H ₂ + He	7.50×10^{-10}	0	0	UDFA06
IM17	He ⁺ + C ₂ H ₂	→	C ₂ ⁺ + H ₂ + He	1.61×10^{-9}	0	0	UDFA06
IM18	He ⁺ + SiO	→	O ⁺ + Si + He	8.60×10^{-10}	0	0	UDFA06
IM19	He ⁺ + SiO	→	Si ⁺ + O + He	8.60×10^{-10}	0	0	UDFA06
IM20	C ⁺ + O ₂	→	CO ⁺ + O	3.80×10^{-10}	0	0	UDFA06
IM21	C ⁺ + O ₂	→	O ⁺ + CO	6.20×10^{-10}	0	0	UDFA06
IM22	C ⁺ + CO ₂	→	CO ⁺ + CO	1.10×10^{-9}	0	0	UDFA06
IM23	C ⁺ + SiO	→	Si ⁺ + CO	5.40×10^{-10}	0	0	UDFA06
IM24	C ⁺ + SO	→	S ⁺ + CO	2.60×10^{-10}	0	0	UDFA06
IM25	C ⁺ + SO	→	CO ⁺ + S	2.60×10^{-10}	0	0	UDFA06
IM26	Si ⁺ + OH	→	SiO ⁺ + H	6.30×10^{-10}	0	0	UDFA06
IM27	S ⁺ + OH	→	SO ⁺ + H	6.10×10^{-10}	0	0	UDFA06
IM28	S ⁺ + O ₂	→	SO ⁺ + O	1.50×10^{-11}	0	0	UDFA06
IM29	C ₂ ⁺ + O	→	CO ⁺ + C	3.10×10^{-10}	0	0	UDFA06
IM30	SiO ⁺ + O	→	Si ⁺ + O ₂	2.00×10^{-10}	0	0	UDFA06
IM31	SiO ⁺ + C	→	Si ⁺ + CO	1.00×10^{-9}	0	0	UDFA06
IM32	SiO ⁺ + CO	→	Si ⁺ + CO ₂	7.90×10^{-10}	0	0	UDFA06
IM33	SiO ⁺ + S	→	Si ⁺ + SO ₂	1.00×10^{-9}	0	0	UDFA06
IM34	SiO ⁺ + N	→	Si ⁺ + NO	2.10×10^{-10}	0	0	UDFA06
CHARGE EXCHANGE							
CE1	H + H ₂ ⁺	→	H ⁺ + H ₂	6.40×10^{-10}	0	0	UDFA06
CE2	O + C ₂ ⁺	→	CO ⁺ + C	3.10×10^{-10}	0	0	UDFA06
CE3	O + CO ⁺	→	O ⁺ + CO	1.40×10^{-10}	0.5	0	UDFA06
CE4	O + C ₂ ⁺	→	CO ⁺ + C	3.10×10^{-10}	0	0	UDFA06
CE5	C + CO ⁺	→	C ⁺ + CO	1.10×10^{-10}	0	0	UDFA06
CE6	C + C ₂ ⁺	→	C ⁺ + C ₂	1.10×10^{-10}	0	0	UDFA06
CE7	C ₂ + O ⁺	→	C ₂ ⁺ + O	4.80×10^{-10}	0	0	UDFA06
CE8	CO + O ⁺	→	CO ⁺ + O	4.90×10^{-12}	0.5	4580.0	UDFA06
CE9	Si + C ⁺	→	Si ⁺ + C	2.10×10^{-9}	0	0	UDFA06
CE10	Si + S ⁺	→	Si ⁺ + S	1.60×10^{-9}	0	0	NIST
CE11	SiO + H ⁺	→	SiO ⁺ + H	3.30×10^{-9}	0	0	UDFA06
CE12	S + C ⁺	→	S ⁺ + C	1.50×10^{-9}	0	0	NIST
CE13	S + CO ⁺	→	S ⁺ + CO	1.10×10^{-9}	0	0	NIST
CE14	Fe + O ⁺	→	Fe ⁺ + O	2.90×10^{-9}	0	0	UDFA06
CE15	Fe + C ⁺	→	Fe ⁺ + C	2.60×10^{-9}	0	0	UDFA06
CE16	Fe + Si ⁺	→	Fe ⁺ + Si	1.90×10^{-9}	0	0	UDFA06
CE17	Fe + S ⁺	→	Fe ⁺ + S	1.80×10^{-10}	0	0	NIST
CE18	Fe + SO ⁺	→	Fe ⁺ + SO	1.60×10^{-9}	0	0	UDFA06
CE19	Mg + H ⁺	→	Mg ⁺ + H	1.10×10^{-9}	0	0	UDFA06
CE20	Mg + O ⁺	→	Mg ⁺ + O	1.10×10^{-9}	0	0	UDFA06
CE21	Mg + C ⁺	→	Mg ⁺ + C	1.10×10^{-9}	0	0	UDFA06
CE22	Mg + Si ⁺	→	Mg ⁺ + Si	2.90×10^{-9}	0	0	UDFA06
CE23	Mg + SiO ⁺	→	Mg ⁺ + SiO	1.00×10^{-9}	0	0	UDFA06
CE24	Al + O ⁺	→	Al ⁺ + O	2.00×10^{-9}	0	0	UDFA06
CE25	Al + C ⁺	→	Al ⁺ + C	2.70×10^{-9}	0	0	UDFA06
CE26	Al + CO ⁺	→	Al ⁺ + CO	2.20×10^{-9}	0	0	UDFA06
CE27	Al + Si ⁺	→	Al ⁺ + Si	2.70×10^{-9}	0	0	UDFA06
CE28	Al + SiO ⁺	→	Al ⁺ + SiO	2.20×10^{-9}	0	0	UDFA06

Table 5
(Continued)

No.	Chemical Processes		A	ν	E_a	Reference ^a	
ELECTRONIC RECOMBINATION							
ER1	$H^+ + e^-$	\rightarrow	H	3.50×10^{-12}	-0.7	0	UDFA06
ER2	$H_2^+ + e^-$	\rightarrow	H + H	1.60×10^{-8}	1.4	0	UDFA06
ER3	$H_3^+ + e^-$	\rightarrow	H ₂ + H	2.34×10^{-8}	-0.5	0	UDFA06
ER4	$H_3^+ + e^-$	\rightarrow	H ₂ + H	2.34×10^{-8}	-0.5	0	UDFA06
ER5	$C^+ + e^-$	\rightarrow	C	4.67×10^{-12}	-0.6	0	UDFA06
ER6	$C_2^+ + e^-$	\rightarrow	C + C	3.00×10^{-7}	-0.5	0	UDFA06
ER7	$CO^+ + e^-$	\rightarrow	C + O	2.00×10^{-7}	-0.5	0	UDFA06
ER8	$O^+ + e^-$	\rightarrow	O	3.24×10^{-12}	-0.7	0	UDFA06
ER9	$Si^+ + e^-$	\rightarrow	Si	4.90×10^{-12}	-0.6	0	UDFA06
ER10	$SiO^+ + e^-$	\rightarrow	Si + O	2.00×10^{-7}	-0.5	0	UDFA06
ER11	$S^+ + e^-$	\rightarrow	S	3.90×10^{-12}	-0.6	0	UDFA06
ER12	$SO^+ + e^-$	\rightarrow	S + O	2.00×10^{-7}	-0.5	0	UDFA06
ER13	$Fe^+ + e^-$	\rightarrow	Fe	3.70×10^{-12}	-0.6	0	UDFA06
ER14	$Mg^+ + e^-$	\rightarrow	Mg	2.80×10^{-12}	-0.9	0	UDFA06
ER15	$Al^+ + e^-$	\rightarrow	Al	3.24×10^{-12}	-0.7	0	UDFA06
COMPTON ELECTRON DESTRUCTION							
CED1	O	\rightarrow	$O^+ + e^-$	1.57×10^{-5}	0	3464.1	See the text
CED2	C	\rightarrow	$C^+ + e^-$	1.99×10^{-5}	0	3464.1	
CED3	Si	\rightarrow	$Si^+ + e^-$	1.57×10^{-5}	0	3464.1	
CED4	S	\rightarrow	$S^+ + e^-$	1.57×10^{-5}	0	3464.1	
CED5	Fe	\rightarrow	$Fe^+ + e^-$	1.57×10^{-5}	0	3464.1	
CED6	Mg	\rightarrow	$Mg^+ + e^-$	1.57×10^{-5}	0	3464.1	
CED7	Al	\rightarrow	$Al^+ + e^-$	1.57×10^{-5}	0	3464.1	
CED8	H ₂	\rightarrow	H + H ⁺ + e ⁻	8.86×10^{-7}	0	3464.1	
CED9	H ₂	\rightarrow	$H_2^+ + e^-$	1.93×10^{-5}	0	3464.1	
CED10	H ₂	\rightarrow	H + H	9.43×10^{-6}	0	3464.1	
CED11	OH	\rightarrow	H + O ⁺ + e ⁻	9.46×10^{-7}	0	3464.1	
CED12	OH	\rightarrow	O + H ⁺ + e ⁻	2.94×10^{-6}	0	3464.1	
CED13	OH	\rightarrow	O + H	5.81×10^{-6}	0	3464.1	
CED14	H ₂ O	\rightarrow	OH + H ⁺ + e ⁻	2.94×10^{-6}	0	3464.1	
CED15	H ₂ O	\rightarrow	OH + H	5.81×10^{-6}	0	3464.1	
CED16	CH	\rightarrow	H + C ⁺ + e ⁻	9.46×10^{-7}	0	3464.1	
CED17	CH	\rightarrow	C + H ⁺ + e ⁻	2.94×10^{-6}	0	3464.1	
CED18	CH	\rightarrow	H + C	5.81×10^{-6}	0	3464.1	
CED19	CH ₂	\rightarrow	CH + H ⁺ + e ⁻	2.94×10^{-6}	0	3464.1	
CED20	CH ₂	\rightarrow	CH + H	5.81×10^{-6}	0	3464.1	
CED21	C ₂ H ₂	\rightarrow	C ₂ H + H ⁺ + e ⁻	2.94×10^{-6}	0	3464.1	
CED22	C ₂ H ₂	\rightarrow	C ₂ H + H	5.81×10^{-6}	0	3464.1	
CED23	HCO	\rightarrow	CO + H ⁺ + e ⁻	2.94×10^{-6}	0	3464.1	
CED24	HCO	\rightarrow	H + CO ⁺ + e ⁻	8.86×10^{-7}	0	3464.1	
CED25	HCO	\rightarrow	H + CO	5.81×10^{-6}	0	3464.1	
CED26	O ₂	\rightarrow	O + O ⁺ + e ⁻	9.46×10^{-7}	0	3464.1	
CED27	O ₂	\rightarrow	O + O	5.81×10^{-6}	0	3464.1	
CED28	CO	\rightarrow	C + O ⁺ + e ⁻	9.46×10^{-7}	0	3464.1	
CED29	CO	\rightarrow	O + C ⁺ + e ⁻	2.94×10^{-6}	0	3464.1	
CED30	CO	\rightarrow	CO ⁺ + e ⁻	2.14×10^{-5}	0	3464.1	
CED31	CO	\rightarrow	C + O	5.81×10^{-7}	0	3464.1	
CED32	CO ₂	\rightarrow	CO + O ⁺ + e ⁻	9.46×10^{-7}	0	3464.1	
CED33	CO ₂	\rightarrow	O + CO ⁺ + e ⁻	2.94×10^{-6}	0	3464.1	
CED34	CO ₂	\rightarrow	CO + O	5.81×10^{-7}	0	3464.1	
CED35	CO ₂	\rightarrow	CO + O ⁺ + e ⁻	9.46×10^{-7}	0	3464.1	
CED36	C ₂	\rightarrow	C + C ⁺ + e ⁻	9.46×10^{-7}	0	3464.1	
CED37	C ₂	\rightarrow	$C_2^+ + e^-$	2.14×10^{-5}	0	3464.1	
CED38	C ₂	\rightarrow	C + C	5.81×10^{-6}	0	3464.1	
CED39	SiO	\rightarrow	Si + O ⁺ + e ⁻	1.07×10^{-7}	0	3464.1	
CED40	SiO	\rightarrow	O + Si ⁺ + e ⁻	3.33×10^{-6}	0	3464.1	
CED41	SiO	\rightarrow	SiO ⁺ + e ⁻	2.42×10^{-5}	0	3464.1	
CED42	SiO	\rightarrow	O + Si	6.58×10^{-6}	0	3464.1	
CED43	SiS	\rightarrow	Si + S ⁺ + e ⁻	2.94×10^{-6}	0	3464.1	
CED44	SiS	\rightarrow	S + Si ⁺ + e ⁻	2.94×10^{-6}	0	3464.1	
CED45	SiS	\rightarrow	Si + S	5.81×10^{-6}	0	3464.1	
CED46	SO	\rightarrow	O + S ⁺ + e ⁻	2.94×10^{-6}	0	3464.1	
CED47	SO	\rightarrow	S + O ⁺ + e ⁻	9.46×10^{-7}	0	3464.1	
CED48	SO	\rightarrow	SO ⁺ + e ⁻	2.14×10^{-5}	0	3464.1	

Table 5
(Continued)

No.	Chemical Processes			A	ν	E_a	Reference ^a
CED49	SO	→	O + S	5.81×10^{-6}	0	3464.1	
CED50	SO	→	O + S ⁺ + e ⁻	2.94×10^{-6}	0	3464.1	
CED51	S ₂	→	S + S ⁺ + e ⁻	9.46×10^{-7}	0	3464.1	
CED52	S ₂	→	S + S	5.81×10^{-6}	0	3464.1	
CED53	N ₂	→	N + N	5.44×10^{-6}	0	3464.1	
UV PHOTODISSOCIATION							
PHOT1	H ₂	→	H + H	3.80×10^{-5}	0	3464.1	See the text
PHOT2	O ₂	→	O + O	3.80×10^{-5}	0	3464.1	
PHOT3	OH	→	O + H	3.80×10^{-5}	0	3464.1	
PHOT4	H ₂ O	→	OH + H	3.80×10^{-5}	0	3464.1	
PHOT5	CO	→	C + O	3.80×10^{-5}	0	3464.1	
PHOT6	CO ₂	→	CO + O	3.80×10^{-5}	0	3464.1	
PHOT7	C ₂	→	C + C	3.80×10^{-5}	0	3464.1	
PHOT8	CO ₂	→	CO + O	3.80×10^{-5}	0	3464.1	
PHOT9	SiO	→	Si + O	3.80×10^{-5}	0	3464.1	
PHOT10	SO ₂	→	S + O	3.80×10^{-5}	0	3464.1	
PHOT11	N ₂	→	N + N	3.80×10^{-5}	0	3464.1	

Notes. Chemical reaction rate coefficients are given according to Equation (7). The Compton electron destruction and UV photodissociation reactions are listed for the 170 M_{\odot} progenitor. Rate values for other progenitors can be derived from Table 6.

^a NIST is the NIST chemical kinetics database. UDFA06 is by Woodall et al. (2007). Other references are listed in the bibliography. “E” means “estimated.”

where κ_{56} is the average γ -ray mass absorption coefficient in $\text{cm}^2 \text{g}^{-1}$, $\phi(t)$ is the mass-column density of the ejecta in g cm^{-2} , $\rho(t)$ and $R(t)$ are, respectively, the mass density and radius of the ejecta at time t , and M_{He} is the mass of the helium core. The average mass absorption coefficient depends on the ejecta composition and the distribution of the radioactive material within the ejecta. For slabs of material consisting of pure He, C, O, Mg, Si, or Fe, $\kappa(E_{\gamma} = 1.25 \text{ MeV}) \approx 0.056 \text{ cm}^2 \text{g}^{-1}$. For the mixed distribution of ^{56}Co in model 10HMM of SN1987A, Woosley et al. (1989) derive an effective value of $\kappa_{56} = 0.033 \text{ cm}^2 \text{g}^{-1}$, which is the value that we will adopt for all models in this paper. Table 1 lists the value of $\tau_0 \equiv \tau(t_0)$, for $t_0 = 100 \text{ d}$, and the relevant parameters used in its calculation, for the different primordial SNe used in this study.

The interaction of the Compton electrons with the molecules leads to their dissociation, ionization, and fragmentation into ionic products. The branching ratios for the different processes depend on W_i , the mean energies per ion-pair for a given species. Available values of W_i for molecules that can form in the ejecta are listed in Table 6. When data are not available, we just assume values similar to those for CO. Using the ^{56}Co mass listed in Table 1 for each progenitor, we calculate the time-dependent rates from Equation (9). However, the rate values need to be expressed under an Arrhenius temperature-dependent form as given by Equation (7). We thus compose the reverse of the time-dependent temperature functions given by Equations (1) and (2) for our modeled ejecta with our rate function given by Equation (9), and derive Compton electron destruction rates as a function of ejecta temperature. We then fit those rates with an Arrhenius function as given by Equation (7). The corresponding Arrhenius parameters are listed in Table 6.

3.1.2. Destruction by UV Radiation

As they slow down in the ejecta, the high-energy Compton electrons deposit their energy in three channels: heating, excitation, and ionization. The ionization of the ejecta by the primary electrons creates secondary fast electrons, which also deposit

their energy in these channels. The fraction of the energy going into each channel depends primarily on the ejecta composition, and on x_e , the electron fraction of the ejecta. Kozma & Fransson (1992; hereafter KF92) calculated these quantities for different ejecta composition as a function of x_e (Figures 3–5 in their paper). Of particular interest to our study is the fraction α of energy that is deposited in the ejecta that emerges as UV radiation. KF92 derived the value of α by calculating the evolution of x_e for different layer compositions thus determining the fractional energy deposited by the high-energy electrons in the different channels as a function of time. They then calculated the amount of UV emission that is released by excitation and ionization in the different composition zones as a function of time. They found that the fraction of the energy that is deposited in the ejecta that emerges as UV photons with wavelengths below 3646 Å is slowly rising from a value of ~ 0.25 on day 200 to ~ 0.4 on day 1000 (Figure 8 in their paper). The destruction rate of molecules by UV photons (in $\text{s}^{-1} \text{molecule}^{-1}$) is thus given by

$$k_{\text{UV}}(i) = \frac{\alpha \times 5.95 \times 10^{53}}{E_{\text{UV}} \times N_i} \left[\frac{M_{56}}{M_{56}(\text{SN1987A})} \right] \times \exp(-t/\tau_{56}) \times (1 - \exp[-\tau_0(t/t_0)^{-2}]), \quad (11)$$

where α is the fraction of deposited energy re-emitted as UV photons, and E_{UV} is the energy of the UV photons. According to FK92, nonthermal excitations and recombinations in the oxygen-rich zone result in emitting OI 1302 Å and 1356 Å photons. We therefore calculate E_{UV} as being the energy of a fiducial photon of wavelength 1302 Å. Other terms are as in Equation (9).

4. RESULTS

In the following sections, we present the abundances and the mass ejected at day 1000 of molecules produced in fully mixed and unmixed ejecta of SNe, excluding those that are dust molecular precursors. Results for gas-phase dust precursors

Table 6

Compton Electron-induced Reactions, Corresponding Mean Energy Per Ion Pair W_i , and Arrhenius Coefficient A as a Function of the Ejecta Model

Species	Reaction	W_i (eV)	$A-20 M_{\odot}^a$	$A-170 M_{\odot}^a$	$A-270 M_{\odot}^a$	Reference
CO	$\rightarrow O^+ + C$	768	1.1610×10^{-7}	9.4576×10^{-7}	1.6741×10^{-6}	Liu & Dalgarno 1995
	$\rightarrow C^+ + O$	247	3.6100×10^{-7}	2.9406×10^{-6}	5.2053×10^{-6}	"
	$\rightarrow C + O$	125	7.1333×10^{-7}	5.8107×10^{-6}	1.0286×10^{-5}	"
	$\rightarrow CO^+ + e^-$	34	2.6225×10^{-6}	2.1363×10^{-5}	3.7815×10^{-5}	"
O	$\rightarrow O^+ + e^-$	46.2	1.9300×10^{-6}	1.5722×10^{-5}	2.7829×10^{-5}	"
C	$\rightarrow C^+ + e^-$	36.4	2.4496×10^{-6}	1.9954×10^{-5}	3.5321×10^{-5}	"
SiO	$\rightarrow O^+ + Si$	678	1.3158×10^{-7}	1.0719×10^{-6}	1.8973×10^{-6}	"
	$\rightarrow Si^+ + O$	218	4.0913×10^{-7}	3.3327×10^{-6}	5.8993×10^{-6}	"
	$\rightarrow Si + O$	110	8.0844×10^{-7}	6.5855×10^{-6}	1.1657×10^{-5}	"
	$\rightarrow SiO^+ + e^-$	30	2.9722×10^{-6}	2.4211×10^{-5}	4.2857×10^{-5}	"
N ₂	$\rightarrow N^+ + N$	264	3.3812×10^{-7}	2.7543×10^{-6}	4.8755×10^{-6}	Khare & Kumar 1977
	$\rightarrow N + N$	133.5	6.6813×10^{-7}	5.4425×10^{-6}	9.6339×10^{-6}	"
	$\rightarrow N_2^+ + e^-$	36.3	2.4564×10^{-6}	2.0009×10^{-5}	3.5419×10^{-5}	"
H	$\rightarrow H^+ + e^-$	36.1	2.4700×10^{-6}	2.012×10^{-5}	3.5615×10^{-5}	Dalgarno et al. 1999
	$\rightarrow H^* (n=2)$	26.6	3.3521×10^{-6}	2.7306×10^{-5}	4.8335×10^{-5}	"
He	$\rightarrow He^+ + e^-$	46.3	1.9258×10^{-6}	1.5688×10^{-5}	2.7769×10^{-5}	"
H ₂	$\rightarrow H^+ + H$	820	1.0874×10^{-7}	8.8578×10^{-7}	1.5679×10^{-6}	"
	$\rightarrow H + H$	77	1.1580×10^{-6}	9.433×10^{-6}	1.6697×10^{-5}	"
	$\rightarrow H_2^+ + e^+$	37.7	2.3651×10^{-6}	1.9266×10^{-5}	3.4103×10^{-5}	"

Note.

^a Arrhenius forms for k_C (see the text): $A \times \exp(-2976.5/T)$ ($20 M_{\odot}$ progenitor) – $A \times \exp(-3464.1/T)$ ($170 M_{\odot}$ progenitor) – $A \times \exp(-5376/T)$ ($270 M_{\odot}$ progenitor).

and small clusters will be presented in a forthcoming paper (I. Cherchneff & E. Dwek 2009, in preparation).

4.1. Ejecta Chemistry is not at Steady State

Previous studies of molecular formation in SN1987A assumed that the chemistry was at steady state, implying that species number densities did not vary with time (Lepp et al. 1990; Liu & Dalgarno 1994, 1995; Gearhart et al. 1999; Clayton et al. 2001). Such assumption was also made by Todini & Ferrara (2001) and SFS04 in their studies of dust formation in primeval SNe. When a small number of chemical reactions are considered, the steady state approximation may be valid, allowing for the direct derivation of analytical solutions for chemical abundances. This assumption requires that at early times, the rates of the chemical reactions be fast compared to the rate of density and temperature changes in the ejecta, so that chemical abundances would quickly reach their equilibrium value. However, fast chemistry does not “a priori” ensure the validity of the steady state approximation in larger chemical systems. Indeed, such large systems bring a greater complexity in terms of chemical rates. Certain species may reach steady state abundances while others are still being formed or destroyed under nonequilibrium conditions.

Figure 2 illustrates this point for the $170 M_{\odot}$ progenitor fully mixed ejecta, by comparing select reaction rates to k_{dyn} , the inverse dynamical timescale, which is defined as

$$k_{\text{dyn}} = \frac{1}{t} = \frac{v}{R(t)}, \quad (12)$$

where v is the ejecta velocity given by Equation (5) and listed in Table 1, and $R(t)$ is the ejecta position at a given time t after explosion. The rates depicted in the figure correspond to those of the major chemical processes involved in the formation and destruction of carbon monoxide, CO. The formation processes

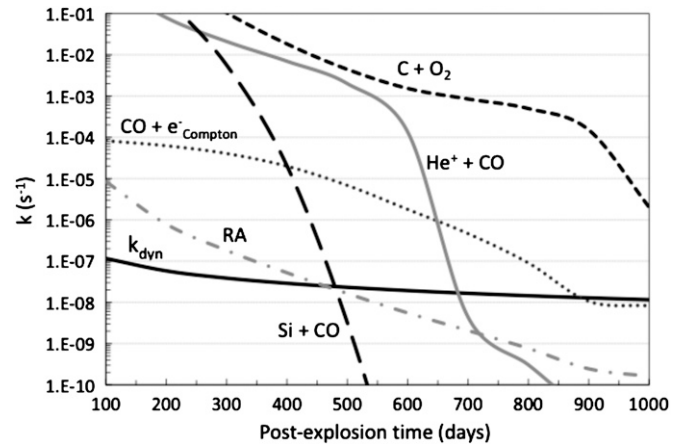
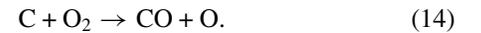


Figure 2. Time dependence of the rates of the major processes leading to the formation of CO (Equations (13)–(17)) is compared to the inverse of the dynamical timescale of the ejecta k_{dyn} for the fully mixed $170 M_{\odot}$ case without hydrogen diffusion. The figure shows when reactions proceed and freeze out, leading to an active chemistry far from steady state.

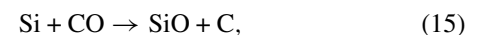
are the radiative association reaction (RA4)



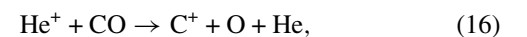
and the bimolecular process (NN56)



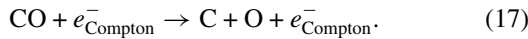
The major CO destruction processes are the bimolecular process (NN70)



the reaction with helium ions (IM13)



and the collision with γ -rays-induced Compton electrons (CED31) given by



We see from Figure 2 that prior to ~ 480 days post-explosion, all reaction rates are larger than the dynamical rate k_{dyn} . A fast chemistry takes place but reactions proceed more or less efficiently, resulting in a nonequilibrium chemistry and a drive toward the formation of molecules. At times greater than 480 days, the RA rate becomes smaller than k_{dyn} and the reaction “freezes” out when bimolecular processes are still active in building up molecules. Compton electron and He^+ reactions are always important in destroying CO up to 900 days and 700 days post-explosion, respectively. Therefore, the relevant processes to CO chemistry are activated and switched off at different times in the ejecta, and the chemistry is by no means at steady-state over the time period of interest. Consequently, molecular abundances show strong variations with time regardless of the initial composition and mixing in the ejecta. This point will be discussed in more detail below.

4.2. Fully Mixed Ejecta

We first consider the chemistry of the fully microscopically mixed helium cores for the primordial SN surrogates under study, exploring the impact of hydrogen mixing on the ejecta chemistry and the dependence of results on the progenitor mass. No UV destruction rates have been included in these models.

4.2.1. Impact of Hydrogen Mixing

Molecular abundances for the $170 M_{\odot}$ surrogate are shown in Figure 3 considering two cases: (a) when no hydrogen is mixed into the He core, and (b) when 10% of the hydrogen mass of the progenitor’s envelope is microscopically mixed uniformly throughout the He core. In the absence of hydrogen, there exist two phases of molecular formation as illustrated in Figure 3(a). The first phase arises at ~ 350 days when three molecules dominate the ejecta: silicon monoxide, SiO, silicon sulfide, SiS, and carbon monoxide, CO. For SiS and CO, the dominant building process is radiative association accounting for more than 94% of the total formation rate, whereas for SiO, RA accounts for only $\sim 56\%$ of the formation rate. The extra formation pathway is the Si reaction with CO leading to the buildup of SiO from CO. Destruction of SiS and SiO occurs through reactions with He^+ at the same time that SiO is being formed by the destruction of CO. At times close to 440 days, silicon-based dust precursors (i.e., small $(\text{SiO})_n$ and $(\text{SiO}_2)_n$ clusters) start forming due to the cooler gas temperatures, and thus deplete Si-bearing molecules and SiO. Reaction with He^+ remains an important destruction channel for SiS, SiO, and CO but for the latter, fast Compton electrons also contribute to the destruction. The second phase of molecular formation starts at ~ 700 days when most of SiO is depleted into dust precursors. CO molecules keep forming from RA and NN reactions involving atomic oxygen and carbon. The formation of O-bearing species such as O_2 and SO are mainly triggered by NN processes involving atomic oxygen and sulfur. Molecular destruction is driven by NN processes as well since He^+ has recombined to neutral and the level of ionization has decreased by a factor of 100 in the ejecta. To summarize, the first phase of molecular formation at high temperatures is triggered by RA processes involving atomic species, whereas the second

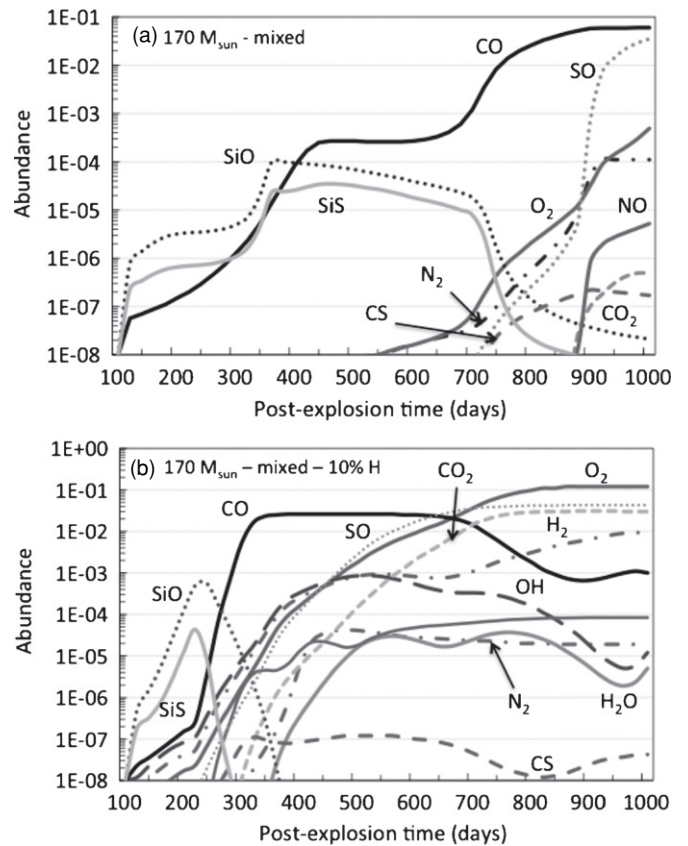


Figure 3. Evolution of molecular abundances normalized to total gas number density for the fully mixed ejecta of the $170 M_{\odot}$ progenitor when no hydrogen mixing is considered (a), and when 10% of the hydrogen mass of the progenitor envelope is microscopically mixed to the helium core (b). The figure illustrates the sensitivity of the chemistry to the presence of hydrogen in the ejecta.

low-temperature phase is driven by NN reactions with small activation energy barriers.

When hydrogen penetration from the progenitor envelope is allowed to a level of 10% of the progenitor hydrogen mass, an active and complex NN chemistry induced by radicals such as OH and CH, comes to play. The radical reservoir is fed by the products of reaction between heavy elements and molecular hydrogen. These radicals boost at early post-explosion times the formation of molecules such as SO, NO, and O_2 , the latter contributing to CO formation via reaction with atomic carbon. Although some of the processes mentioned in the previous section (i.e., reaction with He^+ , RA processes) are still active, the whole kinetics is dominated by NN processes with and without activation energy barriers. Indeed, we see from Figure 3(b) that molecular formation is already fully developed at day 300, converting a large fraction of the ejecta into molecules. After 700 days, CO is converted to CO_2 from its reaction with OH and the ejecta is composed of O_2 , SO, CO_2 , and H_2 . The molecular masses for the dominant species ejected at day 1000 are listed in Table 7 for the fully mixed ejecta as well as the efficiency at forming molecules defined as the ratio of the molecular mass to the helium core mass. For the H-free fully mixed ejecta of the $170 M_{\odot}$ progenitor, the dominant ejected species are CO and SO and the total molecular component of the ejecta equals $\sim 11.3 M_{\odot}$. Defining the molecule formation efficiency as the fraction of the ejected He-core mass that is converted to molecules, we get a formation efficiency of $\sim 13.7\%$. As expected, its H-rich counterpart produces a much larger molecular mass. It chiefly forms O_2 , SO, and CO_2 and the total molecular

Table 7
Mass Yields of Most Important Molecules Ejected at Day 1000 for Fully Mixed Ejecta With and Without Hydrogen Mixing^{a,b}

Molecules	170 M_{\odot}		270 M_{\odot}	20 M_{\odot} ^c
	No Hydrogen	10% Hydrogen	No Hydrogen	No Hydrogen
CO	5.61	0.18	3.22	0.63
SO	5.61	13.28	1.68×10^{-4}	6.35×10^{-2}
O ₂	5.24×10^{-2}	24.71	2.67×10^{-4}	8.79×10^{-2}
CO ₂	7.20×10^{-5}	8.49	3.45×10^{-8}	1.48×10^{-4}
H ₂	0	0.12	0	0
N ₂	1.03×10^{-2}	3.42×10^{-3}	5.70×10^{-4}	2.73×10^{-4}
NO	5.21×10^{-4}	1.62×10^{-3}	1.88×10^{-7}	2.47×10^{-6}
OH	0	1.31×10^{-3}	0	0
Total	11.29	46.80	3.22	0.78
Efficiency	13.71%	56.86%	2.49%	13.42%

Notes.

^a Mass yields are in M_{\odot} .

^b The efficiency is defined as the ratio of the molecular mass to the He core mass.

^c A mass cut of $2.4 M_{\odot}$ is assumed as in Nozawa et al. (2003).

mass is $\sim 47 M_{\odot}$, corresponding to a formation efficiency of $\sim 57\%$.

Models assuming fully microscopically mixed ejecta are highly unrealistic, since observations of young SN remnants show that their ejecta are unmixed. Our purpose in admixing H is to illustrate the paramount effect of hydrogen on molecular synthesis in the ejecta. Hence, any hydrogen that microscopically mixes with nearby heavy elements at the interface of finger structures and inhomogeneities should induce efficient synthesis of H-bearing radicals and molecules. Conversely, He⁺ is detrimental to molecular formation, as first stressed by Lepp et al. (1990) in their attempt to modeling CO in SN1987A. Indeed, its attack represents one of the principal destruction channels to molecules, whereas attack by Compton electron always plays a minor role. This may not be the case for the unmixed ejecta, as discussed in the following section.

4.2.2. Impact of Progenitor Mass

We now turn to study the impact of the progenitor mass on the ejecta chemistry. We consider a massive progenitor surrogate of mass $270 M_{\odot}$ so that we can directly compare results to those obtained in the previous section for the $170 M_{\odot}$ PISN progenitor. We also consider a CCSN with a $20 M_{\odot}$ progenitor to see if lower mass ejecta can efficiently form a molecular phase or not. As shown in Tables 1 and 2, different masses for Pop III stars imply different initial chemical compositions, explosion energies, ejection velocities, gas temperatures, and number densities. The gas column depths and opacities will change too, resulting in the Compton electron destruction rates listed in Table 2. In both cases, no hydrogen penetration into the helium core is included. Molecular abundances with respect to total gas number density are presented in Figure 4.

From the comparison of Figures 4 and 3, we see that the same species form in the $170 M_{\odot}$ and the $270 M_{\odot}$ ejecta. However, molecular formation is delayed for the more massive ejecta to day 550 primarily due to the higher gas temperatures. The chemical processes at play are identical to those mentioned in Section 4.2.1. SiO is too depleted on day 500 at the onset of dust precursor nucleation. As to molecular abundances, they are globally lower for the $270 M_{\odot}$ progenitor due to a less favorable initial chemical composition of the ejecta gas at 100 days post-explosion. Indeed, we see from Table 2 that the mass of helium (and thus He⁺) relative to the total progenitor mass is larger for the $270 M_{\odot}$ surrogate compared to the $170 M_{\odot}$ progenitor. The

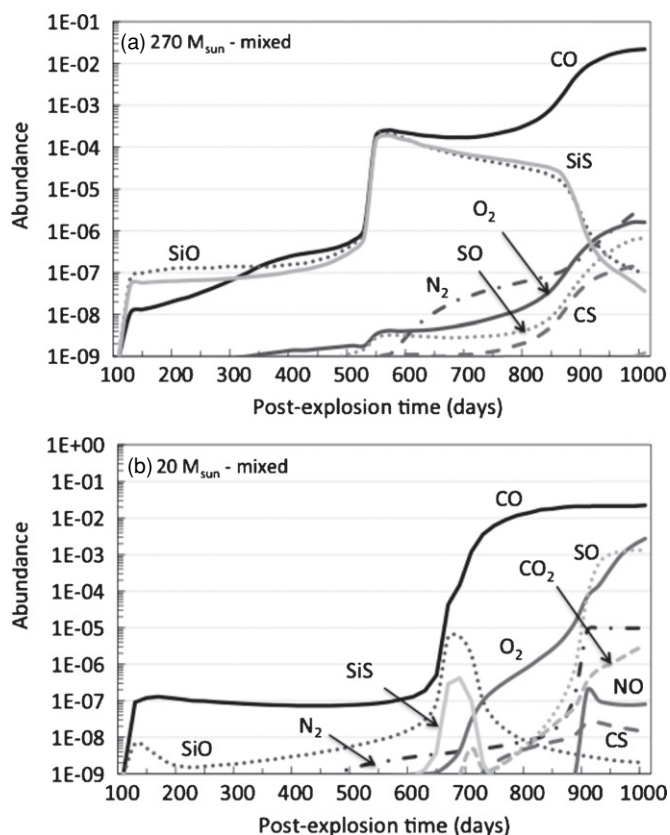


Figure 4. Evolution of the molecular abundances normalized to total gas number density for the fully mixed ejecta: (a) $270 M_{\odot}$ progenitor; (b) $20 M_{\odot}$ progenitor. No hydrogen mixing is considered in both cases.

oxygen and carbon contents are also lower, resulting in smaller CO abundances in the ejecta. These conditions conspire to delay the formation of molecules, which consequently takes place at lower gas densities resulting in lower formation efficiencies. The results are summarized in Table 7 which compares the molecular yield of the $170 M_{\odot}$ and the $270 M_{\odot}$ PISNe without and with hydrogen mixing. Therefore, low-mass PISNe coming from Pop III progenitors should form more molecules in their ejecta than their very massive counterparts.

It is of interest to compare the present results for the $170 M_{\odot}$ and $270 M_{\odot}$ surrogates to the study of dust formation in the fully mixed ejecta of PISN by SFS04. Their modeling of dust

formation accounts for the formation of CO and SiO following the formalism of Todini & Ferrara (2001). However, both studies derive CO and SiO masses assuming those molecules form at steady state, and consider only one formation channel (RA reaction) and one destruction channel via collision with Compton electrons. SFS04 derive a total CO mass of ~ 6 and $0.01 M_{\odot}$ in the ejecta of the $170 M_{\odot}$ and $260 M_{\odot}$ PISN, respectively, but they do not show the evolution of molecular mass with time. In our model, the CO mass ejected at 1000 days after the explosion of the $170 M_{\odot}$ progenitor is $5.8 M_{\odot}$, seemingly in good agreement with the SFS04 value. However, we ascribe this result to pure coincidence, since the chemical approaches and physical models used in our studies are totally different from theirs. In particular, SFS04 assume much lower temperatures in their PISN ejecta than ours. Furthermore, their initial carbon yield is that of Heger & Woosley (2002) which is twice as large as our initial carbon mass taken from Umeda & Nomoto (2002), suggesting a lower CO formation efficiency in their model. There is also a great discrepancy between the CO yield calculated by SFS04 for their $260 M_{\odot}$ progenitor, and our CO yield for the $270 M_{\odot}$ progenitor, which is about 300 times larger. We see from Figure 4 that CO formation proceeds at times greater than 500 days via non-steady-state chemistry. NN bimolecular processes such as the reaction of atomic carbon with molecular oxygen commands CO formation, whereas the dominant destruction channel is He^+ attack. These mechanisms are not considered in the SFS04 study. All shortcomings in the SFS04 models point out the importance of using a kinetic approach to *both* processes, the synthesis of molecules and the nucleation of dust in the ejecta. The two are intrinsically linked, since the formation of molecules (that are not dust precursors) depletes the ejecta from refractory elements that would otherwise be included in the dust formation process.

In the $20 M_{\odot}$ case, molecular formation patterns are quite different. On the one hand, the lower ejecta temperatures foster molecular synthesis. On the other hand, the large helium content of the ejecta and the resulting higher He^+ abundances efficiently inhibit molecule production. The initial elemental composition also implies less refractory elements such as Si or Mg available for the formation of molecules and the nucleation of metal oxides. The combination of the paucity of refractory elements and the elevated He^+ abundances at times less than 700 days explain the low molecular abundances, as illustrated in Figure 4. Once He^+ has recombined at late times, the formation of molecules such as CO, SO, and O_2 can proceed. We see from Table 7 that the fully mixed ejecta of CCSNe are as efficient as their massive counterparts at synthesizing molecules at late post-explosion times.

4.3. Unmixed Ejecta

As stressed in the previous section, it is unlikely that SN ejecta are fully microscopically mixed. We thus consider totally unmixed ejecta in which each mass zone of the helium core has retained the stratified pre-explosive stellar composition, except for the innermost mass zone whose composition reflects the explosion nucleosynthesis. We further assume that the elements are microscopically mixed within each mass zone. Results for the unmixed ejecta of two “primordial” SNe, one $170 M_{\odot}$ PISN and a $20 M_{\odot}$ CCSN, are presented in the following sections. The zoning and initial elemental compositions are those of Table 3, and we explore the impact on the chemistry of a secondary UV field as defined in Section 3.1.2.

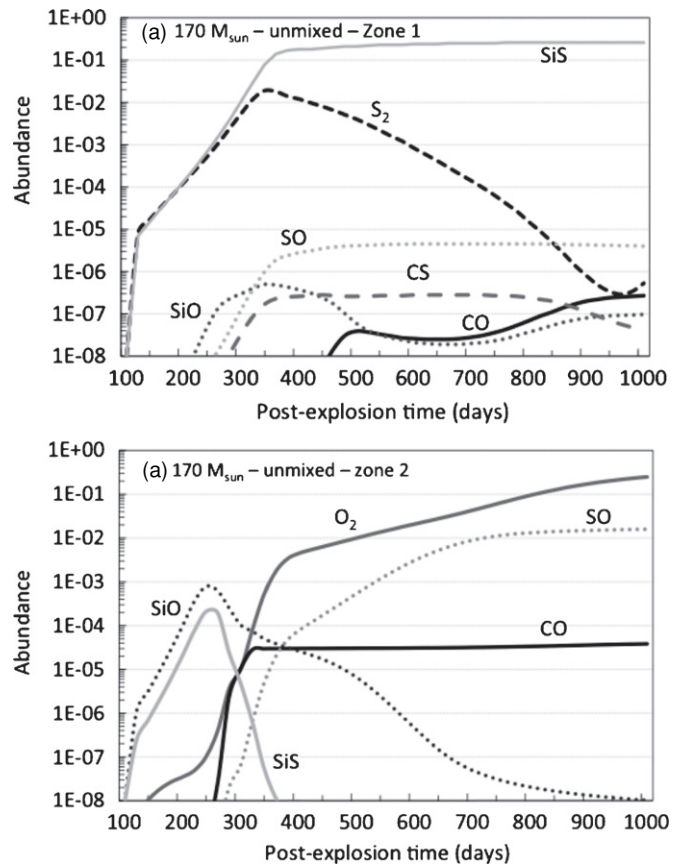


Figure 5. Evolution of the molecular abundances normalized to total gas number density for the $170 M_{\odot}$ unmixed ejecta: (a) the Si/S/Fe-rich zone 1; (b) the O/Si/Mg/S-rich zone 2.

4.3.1. $170 M_{\odot}$ Ejecta: Impact of UV Radiation

Molecular abundances normalized to the total gas number density are shown in Figure 5 for zones 1 and 2, in Figure 6 for zones 3 and 4, and in Figure 7 for zone 5. In zone 1, the formation of S_2 is coupled to that of SiS and FeS. The major formation process for SiS is the NN72 reaction $\text{S}_2 + \text{Si} \rightarrow \text{SiS} + \text{S}$, while the RA reaction between atomic S and Si contributes to a lesser extent. The reverse reaction of the NN channel is actually the major formation process for S_2 . However, since the initial mass of Si is four times larger than that of S, the net formation of SiS is always more efficient than that of S_2 . After ~ 350 days, the reservoir of S_2 is depleted through the continuous formation of SiS and the simultaneous formation of FeS, the molecular precursor to iron sulfide clusters, through the reaction of Fe with S_2 (see Figure 5(a)). As a result, SiS is the most abundant molecule formed in zone 1.

In zone 2, most molecules are rapidly formed from RA processes, whereas thermal fragmentation is the dominant destruction process at early times, due to the high gas temperatures. O_2 and SiO formation are coupled, for O_2 is partly destroyed by the NN69 reaction with atomic Si to form SiO. At ~ 250 days post-explosion, Si and SiO abundances decrease due to nucleation of silica dust precursors such as $(\text{SiO})_n$, resulting in a sharp increase of O_2 abundance. As SO and CO are also formed in the NN reaction of O_2 with S and C atoms (reactions NN76 and NN56, respectively), their abundances show a steep rise with increasing O_2 . The low amount of CO formed in the gas is due to the initial low carbon content of this mass zone.

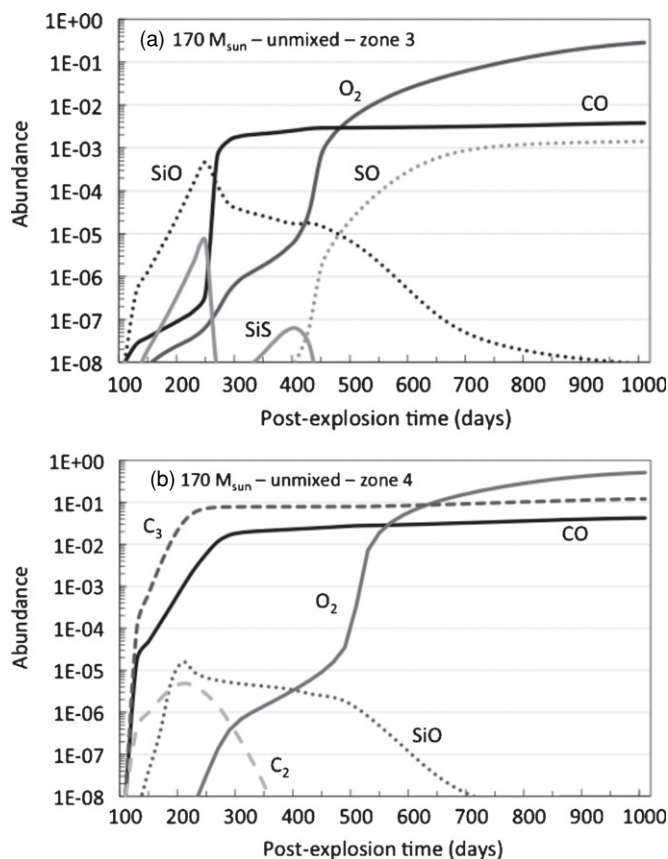


Figure 6. Evolution of the molecular abundances normalized to total gas number density for the $170 M_{\odot}$ unmixed ejecta: (a) the O/Mg/Si-rich zone 3; (b) the O/C/Mg-rich zone 4 in which the rapid conversion of CO to C_2 take place despite a C/O ratio of 0.29.

The chemical processes pertaining to zone 2 also apply to zone 3 and the resulting molecules are similar to those of zone 2, as seen in Figure 6(a). The differences in abundance variation and magnitude with time are due to the different initial chemical composition of zone 3. Specifically, the higher carbon initial mass yield drives the formation of CO via RA process at early times, depleting some of the atomic oxygen available to the formation of O_2 and resulting in higher CO abundances and lower O_2 and SO abundances over time than in zone 2.

Despite the fact that zone 4 is oxygen-rich, it is characterized by high initial carbon mass compared to zones 2 and 3 (see Table 3). However, it is expected that its initial chemical composition precludes the formation of carbon-rich molecules other than CO as its C/O ratio is ~ 0.29 . However, we see from inspection of Figure 6(b) that very early on C_2 and C_3 form in large amounts. This carbon chain formation is a consequence of the thermal fragmentation of CO at very high temperatures and its rapid conversion to C_2 . Indeed, fragmentation studies of CO in shock tube experiments at temperatures between 5000 K and 18,000 K show that C_2 and electronically excited CO^* are always detected along with the collisional destruction of CO in the high-temperature post-shock gas (Fairbairn 1968; Appleton et al. 1970; Hanson 1973). This is readily explained by the following chemical mechanism (labeled TF13, NN57, and TF18 in Table 5):

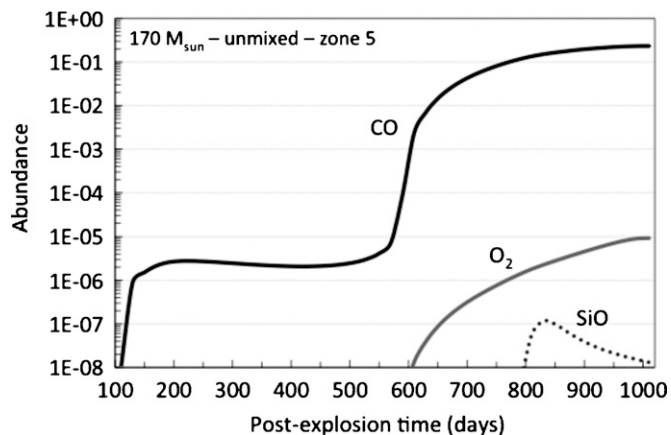


Figure 7. Evolution of the molecular abundances normalized to total gas number density in the O/C/He-rich zone 5 of the $170 M_{\odot}$ unmixed ejecta. CO is the only molecule to form due to the destruction of molecules by He^+ .

and



where M is the colliding buffer gas (chosen as Ar, O, C, or CO in shock tube experiments), and all reactions and their reverse processes occur simultaneously. We see that along with the destruction of CO by collision with M, its rapid conversion to C_2 occurs through reaction with atomic carbon (Equation (19)). Chemical rates characterizing these reactions have high activation energy barriers and thus only proceed at high temperatures. Indeed, at temperatures less than 5000 K, rates for reactions (18), (19), and (20) become small. As to C_3 , the buildup of the end-product of the carbon chains is due to its formation from reaction of two C_2 molecules which rapidly depletes C_2 chains from the gas, as seen in Figure 6(b). A carbon dust mass yield cannot be derived from the C_3 abundance profile, for the formation of C-bearing large chains and rings has not yet been included in the chemical network. It is expected that C_3 will be transformed in larger carbon chains and that atomic oxygen in the gas will partly destroy those chains through the formation of CO. Therefore, carbon chain abundances should be smaller than values for C_3 derived in this study. However, the quick conversion of CO into C_2 will keep triggering the buildup of carbon dust molecular precursors in this O-rich mass zone. Two rates are reported in the literature for the $C + CO$ reaction: a fast rate calculated by Fairbairn (1968) and Hanson (1973), which we use in our ejecta model, and a value listed in the UDFA06 database but with no traceable reference (Woodall et al. 2007). The latter is ~ 10 times smaller than the former. We ran the full model for zone 4 including the lowest rate and find that the C_3 abundance at day 1000 is decreased by a factor of 3, the CO abundance is increased by a factor of 6, and the O_2 abundance is decreased by 30% compared to the values illustrated in Figure 6(b). In both cases, however, the quick CO conversion to C_2 via the $C + CO$ reaction observed in thermal fragmentation experiments is a “natural” mechanism to produce carbon-bearing species and carbon dust in a hot, oxygen-rich environment where carbon is initially in atomic form. When CO conversion to C_2 is not considered, no C_2 forms in large enough quantities to provide significant amounts of the end-product carbon chain C_3 .

To account for the formation of carbon dust in CCSNe, Clayton et al. (1999, 2001) proposed that CO dissociates in a fully mixed ejecta from collisions with Compton electrons and reactions with He^+ . The chemistry is assumed to be at

Table 8
Mass Yields of Most Important Molecules Ejected at Day 1000 for the Unmixed Ejecta of the $170 M_{\odot}$ Progenitor Without Hydrogen Mixing^{a,b}

Zone Mass	Zone 1	Zone 2	Zone 3	Zone 4	Zone 5	Zone 1-5
Zone C/O	($20 M_{\odot}$)	($20 M_{\odot}$)	($15 M_{\odot}$)	($23 M_{\odot}$)	($4.3 M_{\odot}$)	($82.3 M_{\odot}$)
	0.066	2.9×10^{-5}	0.03	0.29	0.56	
O ₂	0	6.24	5.98	13.80	9.28×10^{-5}	26.00
SiS	7.36	0	0	8.79×10^{-6}	0	7.36
CO	0	8.39×10^{-4}	6.98×10^{-2}	9.95×10^{-1}	2.03	3.09
SO	9.06×10^{-5}	5.97×10^{-1}	4.47×10^{-2}	0	0	0.64
Total mass	7.36	6.84	6.10	14.80	2.03	37.09
Efficiency	41.81%	34.18%	40.64%	64.22%	47.21%	45.07%

Notes.

^a Mass yields are in M_{\odot} .

^b The efficiency is defined as the ratio of the molecular mass to the zone mass.

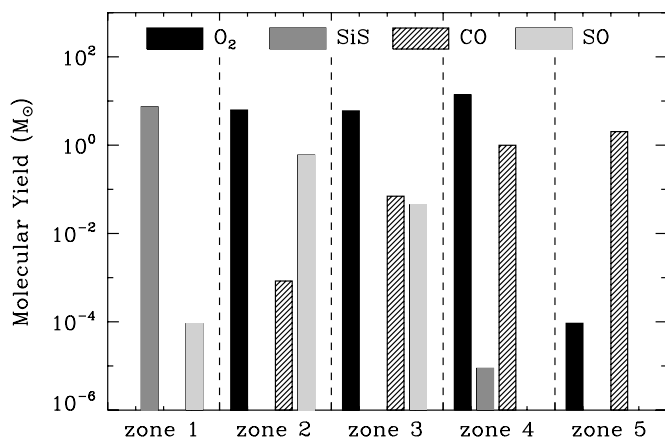


Figure 8. Mass yield (in M_{\odot}) of molecules ejected at day 1000 for the unmixed ejecta of the $170 M_{\odot}$ progenitor.

steady state and CO dissociation creates a pool of carbon atoms from which carbon chains and solid clusters can nucleate and condense. However, we see from Sections 4.1 and 4.2 that under non-steady-state conditions, the two mechanisms invoked by Clayton et al. do not succeed in destroying enough CO to provide free carbon atoms. Indeed, for the three hydrogen-free mixed ejecta, CO is always the dominant species synthesized in the gas. Furthermore, He^+ being a predator to molecules at early times, CO formation is delayed to post-explosion times characterized by temperatures low enough to preclude the quick CO conversion to C_2 from operating. We conclude that fully mixed SN ejecta cannot form free atomic carbon and carbon-based solids in general. Conversely, unmixed SN ejecta, in particular He-free zones where oxygen is more abundant than carbon, can generate carbon chains from the quick conversion of CO through the $\text{C} + \text{CO}$ reaction operating at high temperatures. As to prevalent chemical formation processes in zone 4, we find that both RA reactions and NN bimolecular routes are active at high temperatures to forming species which are destroyed by thermal fragmentation reactions. Molecular formation and destruction in the intermediate temperature regime (1000–5000 K) are too governed by NN bimolecular reactions when destruction via collisions with Compton electron also participates but to a much less extent.

As to zone 5, we see from Figure 7 that the major molecule to form is carbon monoxide. In the outer zone, the formation of He^+ at early times triggers the simultaneous formation of ions such as O^+ and C^+ . NN processes are then not as important as they are in other zones for the formation of molecules. This fact,

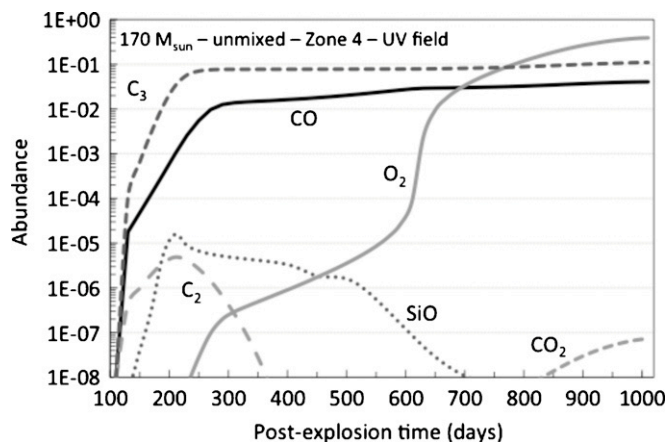


Figure 9. Evolution of the molecular abundances normalized to total gas number density for zone 4 of the $170 M_{\odot}$ unmixed ejecta where UV radiation is included. Molecular abundances are quasi similar to those in Figure 6 except for O_2 whose formation is delayed to later times due to UV destruction.

combined with the destruction of species by He^+ , hampers the effective formation of molecules over most of the post-explosion times. CO, and to a less extent O_2 , thus form at late times after He^+ recombination.

The molecular masses ejected at day 1000 are summarized for all zones in Table 8 and illustrated in Figure 8. The efficiencies listed are defined as the ratio of the molecular mass formed per zone to the zone mass. The value in the last column corresponds to the total molecular mass formed in the unmixed ejecta divided by the summed mass of the zones. In the unmixed case, molecules reflect the chemical composition of the zone in which they form. Dioxygen O_2 is by far the most abundant species in the ejecta and form efficiently in three mass zones when SiS too forms in large amount but is confined to the innermost region of the He core. The final molecular content of the ejecta equals $\sim 37.1 M_{\odot}$, and the total formation efficiency is 45.07%, a very high value. This means that massive PISNe are effective at converting almost half of their initial atomic content into a molecular phase. This value is much larger than that for the fully microscopically mixed case without hydrogen mixing. This result once again illustrates the primary role of He^+ in impeding the formation of molecules.

The impact of the UV field as described in Section 3.1.2 is explored for zone 4 which produces the largest amount of molecules. The results on molecule abundances are shown in Figure 9. Formation and destruction processes for the dominant species are similar to those when no UV field is considered.

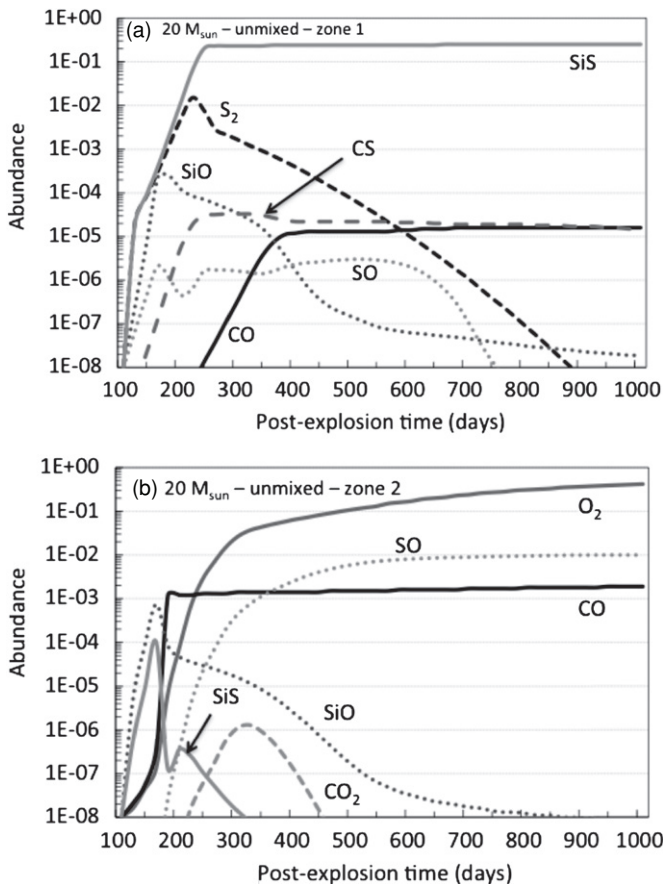


Figure 10. Evolution of the molecular abundances normalized to total gas number density for the $20 M_{\odot}$ unmixed ejecta: (a) the Si/S/Fe-rich zone 1; (b) the O/Si/Mg/S-rich zone 2.

While thermal fragmentation and NN bimolecular reactions remain the dominant destruction processes at high temperatures, molecular destruction by UV becomes effective at times greater than \sim day 350, reducing the abundances of some important molecules. Specifically, O_2 is affected as its formation is postponed to later times, as seen in Figure 9. The final O_2 abundance at day 1000 is decreased by 30% compared to its value when no UV radiation is considered. However, the overall major chemical processes involved in molecular synthesis remain identical. We also consider UV photodissociation in our fully mixed SN ejecta and find that the impact of UV photodissociation is minor compared to the destruction of chemical species by He^+ . We thus conclude that UV photoprocesses if present have some minor impact as destruction channels to molecules and that their effect on the overall chemistry of the ejecta is limited.

4.3.2. $20 M_{\odot}$ Ejecta

We now turn to studying the unmixed ejecta of a zero-metallicity, $20 M_{\odot}$ progenitor core-collapse supernova. Results for zones 1, 2, and 3 as defined in Table 3 are presented in Figures 10 and 11. These zones provide most of the molecules in the ejecta as seen from Table 9, which gives the total molecular masses formed in each zone at day 1000. These mass yields are illustrated in Figure 12.

The chemical processes which occur in zone 1 are similar to those at play in zone 1 of the $170 M_{\odot}$ unmixed ejecta, resulting in the ejection of large amounts of SiS a day 1000. However, large amounts of oxygen and carbon compared to silicon and sulfur are initially presented in the initial composition of the $20 M_{\odot}$

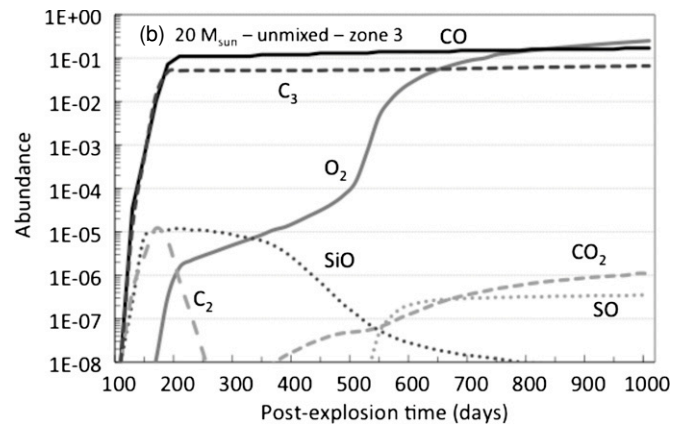


Figure 11. Evolution of the molecular abundances normalized to total gas number density for the O/C/Mg-rich zone 3 of the $20 M_{\odot}$ unmixed ejecta. The rapid conversion of CO to C_2 takes place despite a C/O ratio of 0.33.

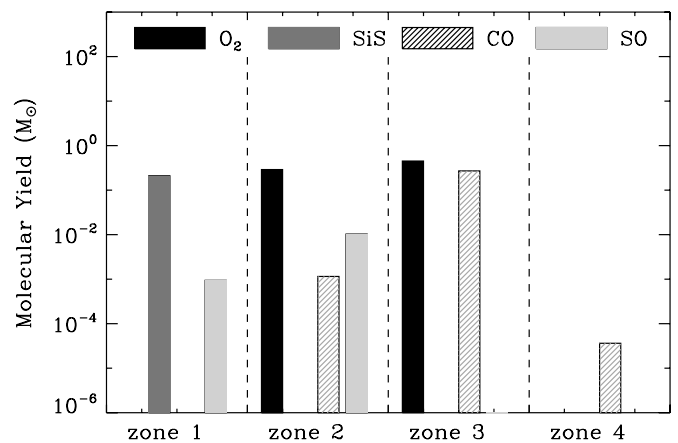


Figure 12. Mass yield (in M_{\odot}) of molecules ejected at day 1000 for the unmixed ejecta of the $20 M_{\odot}$ progenitor.

CCSN, resulting in an active carbon chemistry. For example, CS forms in large quantities from the reaction of atomic C with S_2 and CO abundances are too enhanced compared to zone 1 of the $170 M_{\odot}$ ejecta.

The chemistry of zone 2 is similar to that at play in zone 2 of the $170 M_{\odot}$ PISN, that is, early formation of most molecules by RA reactions and destruction by thermal fragmentation, and coupled chemical processes for the formation of O_2 , SiO, CO, and SO at later times. The dominant species ejected at day 1000 are O_2 , SO, and CO, as illustrated in Figure 10(b).

Zone 3 can be compared to zone 4 of the $170 M_{\odot}$ progenitor case as both zones are characterized by a C/O ratio less than 1 (0.33 and 0.29 for the $20 M_{\odot}$ zone 3 and the $170 M_{\odot}$ zone 4, respectively) and are helium-free. Similar chemical processes are effective at building up molecules in both zones. The rapid conversion of CO to C_2 once again triggers the formation of carbon chains in zone 3 but the overall process is less efficient than for the $170 M_{\odot}$ progenitor owing to the lower temperatures in the ejecta. This is illustrated in Figure 10(b) where CO always remains more abundant than the carbon-chain end product C_3 , and is gradually converted into O_2 at late post-explosion times by its reaction with atomic oxygen.

In zone 4, characterized by a large He mass and a C/O ratio of 29.5, the mass of molecules formed is negligible as seen from Table 9. This is primarily due to the initial chemical composition of the zone where more than 98% of the mass is helium, while C and O only represent 1.7% and 0.08% of the zone mass,

Table 9
Mass Yields of Most Important Species Ejected at Day 1000 for the Unmixed Ejecta of the $20 M_{\odot}$ Progenitor Without Hydrogen Mixing^{a,b}

Zone Mass	Zone 1	Zone 2	Zone 3	Zone 4	Zones 1–4
Zone C/O	$(0.6 M_{\odot})^c$	$(0.6 M_{\odot})$	$(1.35 M_{\odot})$	$(0.9 M_{\odot})$	$(3.45 M_{\odot})$
	0.013	0.0013	0.33	29.47	
O ₂	0	0.29	0.45	0	0.74
CO	0	1.15×10^{-3}	0.27	3.63×10^{-5}	0.27
SiS	0.21	0	0	0	0.21
SO	9.43×10^{-4}	1.03×10^{-2}	9.49×10^{-7}	0	0.01
Total mass	0.21	0.3	0.72	0	1.23
Efficiency	35.37%	50.14%	53.41%	0.004%	35.75%

Notes.

^a Mass yields are in M_{\odot} .

^b The efficiency is defined as the ratio of the molecular mass to the zone mass.

^c A mass cut of $2.4 M_{\odot}$ is assumed for zone 1 as in Nozawa et al. (2003).

respectively. Molecules once formed are chiefly destroyed by He^+ at any times in the ejecta owing to its overwhelming presence.

Table 9 and Figure 12 show that low-mass, zero-metallicity progenitors are almost as efficient at forming a molecular phase in their ejecta than their massive counterparts. The total efficiency at forming molecules is 35.65%, a slightly lower value than that of the $170 M_{\odot}$ case. This lower efficiency is primarily due to the $20 M_{\odot}$ zone 4, which, as discussed above, does not form molecules.

5. SUMMARY AND DISCUSSION

We have investigated the chemistry of the ejecta of Pop III progenitor SNe and find that copious amounts of molecules form in these inhospitable environments. Of particular importance are the following points.

1. As already stated by CL08, the chemistry in SN ejecta is not at steady state from 100 to 1000 days after explosion. New chemical channels involving neutral–neutral processes prevail over radiative association reactions, Compton electron destruction routes, and photodissociation by ambient UV photons. Ion–molecule reactions play a role at late times when the ejecta is cool and diffuse. Our results for relevant molecules such as CO or SiO disagree with existing studies due to the fact that the chemistry is not at steady state. We find that the chemistry of Pop III SN ejecta, owing to the large ranges of temperatures and densities spanned over relatively short times, is complex, manifold, and conducive to molecule synthesis.
2. A new pathway to the formation of carbon chains is active in the oxygen-rich mass zone of the unmixed ejecta and is identified as the CO conversion to C_2 via collision with C. This fast conversion is usually observed in the thermal fragmentation of carbon monoxide in high-temperature shock tube experiments. When this conversation is suppressed, no carbon-bearing molecules and chains are formed. Thus, this conversion channel triggers the formation of carbon chains and dust in an oxygen-rich gas. It is then relevant to any gaseous O-rich environment characterized by high temperatures ($T > 5000$ K) and a large atomic carbon fraction.
3. The present results are extremely sensitive to mixing in the ejecta. We find that the injection of hydrogen from the progenitor envelope in fully mixed ejecta boosts molecular synthesis via the formation of radicals like OH. This result

too applies to unmixed ejecta. On the other hand, we show that helium severely hampers the formation of molecules through He^+ attack. Therefore, the detection of molecules in SN ejecta brings evidence for the non-mixing of helium with other elements in the ejecta gas.

4. The results of our calculations show that the fully mixed $170 M_{\odot}$ and $270 M_{\odot}$ progenitors produce $11 M_{\odot}$ and $3.2 M_{\odot}$ of molecules, respectively. Therefore, a larger progenitor mass does not imply a larger molecular content of the ejecta. This is chiefly due to the harsh physical conditions encountered in the ejecta of the $270 M_{\odot}$ progenitor and to its initial chemical composition. Indeed, although the $270 M_{\odot}$ model is characterized by larger heavy element masses with respect to its $170 M_{\odot}$ counterpart, its helium mass is almost three times greater than that of the $170 M_{\odot}$ case, implying efficient destruction of molecules. The admixing of 10% of the hydrogen present in the $170 M_{\odot}$ progenitor envelope into the fully mixed ejecta dramatically increases its molecular yield to $\sim 47 M_{\odot}$. The more realistic unmixed ejecta of a $170 M_{\odot}$ progenitor supernova synthesizes $\sim 37 M_{\odot}$ of molecules at post-explosion day 1000, which is significant. About half of the initial elemental content of the He core is converted into molecules. The most abundant species by mass is O₂ followed by SiS, CO, and SO. Its $20 M_{\odot}$ counterpart produces $\sim 1.2 M_{\odot}$. O₂ is the dominant species followed by CO, SiS, and SO. This lower efficiency at forming chemical species for the low-mass CCSN is due to the existence of its extended helium-rich outer zone in which molecular synthesis is suppressed.
5. The present results hold for Pop III SNe but the large mass yields of molecules formed in their ejecta address the possibility of potential observational detection of new molecules in nearby SN ejecta. As stated above, our primordial $20 M_{\odot}$ progenitor forms O₂, CO, SiS, and SO shortly after explosion. CO and SiO have already been detected at IR wavelengths in several SN ejecta. However, molecules such as SiS and O₂ are tracers of stratified, unmixed ejecta, while microscopic mixing with hydrogen produces tracer species such as CO₂, OH, and H₂O. Search for those chemical species should be undertaken at IR and submillimeter wavelengths.

The large amounts of molecules synthesized in the PISN ejecta are exposed to a harsh environment generated by the PISN blast wave. The shock expanding into the ambient circumstellar/interstellar medium generates fast particles that are

accelerated to cosmic-ray energies. These penetrate the cavity generated by the blast wave subjecting the ejecta to the constant bombardment by high-energy electrons and nuclei. The pressure of the material that is shock-heated by the advancing blast wave will generate a reverse shock that will move into the expanding PISN ejecta (e.g., Nozawa et al. 2007). Locally, observations of young supernova remnant, such as Cas A, show that their ejecta is very clumpy, the clumps consisting of X-ray filaments with densities $\sim 1\text{--}10\text{ cm}^{-3}$, and optical- and IR-line emitting knots with densities of $\sim 10^3\text{--}10^4\text{ cm}^{-3}$ (Fesen et al. 2006; Smith et al. 2009). Therefore, the fate of the ejected molecules will depend on their environment. Low-density filaments are heated by the reverse shock to X-ray emitting temperatures. Chemical species are not likely to survive this harsh environment. The dust and molecules inside the optical- and IR-line emitting clumps will encounter a much slower shock. Their fate will depend on the relative timescales of many different processes operating in the cavity of the young remnant: the radiative cooling time of the shocked clump, the timescales for the heating of the clump by thermal conduction and ambient cosmic rays, the evaporation timescale of the clump, and the timescale for the development of various instabilities that can lead to its fragmentation and subsequent evaporation. Any surviving molecules will be further subjected to the general diffuse interstellar UV radiation field generated by the Pop III stars. It is therefore very unlikely that the molecules synthesized in the Pop III SN ejecta will have any global cosmological impact. However, they can have a significant local impact. The expanding PISN blast wave will generate during the radiative phase of its evolution a cold dense shell. This shell may be subject to various instabilities that can cause its collapse, forming the next generation of stellar objects (MacKey et al. 2003; Schneider et al. 2006). These stars, commonly referred to as Pop 2.5 stars, will form out of a gas that contains an admixture of the heavy elements, molecules, and dust that formed in the PISN ejecta. The mass of these stellar objects will depend on their ability to fragment into smaller structures, which is greatly facilitated by the cooling rate of the gas via atomic and molecular processes, and by the conversion of the cloud's internal energy to IR emission by dust (Bromm & Larson 2004). The survival of the molecules and dust, and their effect on the formation of stars in this propagating star formation scenario will be explored in a subsequent paper.

I.C. acknowledges support from the Swiss National Science Foundation through a Maria Heim-Vögtlin fellowship.

REFERENCES

- Abel, T., Bryan, G. L., & Norman, M. L. 2002, *Science*, 295, 93
 Andreezza, C. M., & Marinho, E. P. 2005, *ApJ*, 624, 1121
 Andreezza, C. M., & Marinho, E. P. 2007, *MNRAS*, 380, 365
 Andreezza, C. M., Singh, P. D., & Sanzovo, G. C. 1995, *ApJ*, 451, 889
 Appleton, J. P., Steinberg, M., & Liquornik, D. J. 1970, *J. Chem. Phys.*, 52, 2205
 Arnett, W. D. 1988, *ApJ*, 331, 377
 Arnett, W. D., & Fu, A. 1989, *ApJ*, 340, 396
 Babb, J. F., & Dalgarno, A. 1995, *Phys. Rev. A*, 51, 3021
 Bandiera, R. 1984, *A&A*, 139, 368
 Beelen, A., et al. 2006, *ApJ*, 642, 694
 Benz, W., & Thielemann, F.-K. 1990, *ApJ*, 348, 17
 Bertoldi, F., et al. 2003, *A&A*, 406, 55
 Bromm, V., Coppi, P. S., & Larson, R. B. 2002, *ApJ*, 564, 23
 Bromm, V., & Larson, R. B. 2004, *ARA&A*, 42, 79
 Burrows, A., & van Riper, K. A. 1995, *ApJ*, 455, 215
 Catchpole, R. M., et al. 1988, *MNRAS*, 231, 75
 Cherchneff, I., & Lilly, S. 2008, *ApJ*, 683, L123 (CL08)
 Chevalier, R. A. 1976, *PASP*, 88, 588
 Clayton, D. D., Deneault, E. A.-N., & Meyer, B. S. 2001, *ApJ*, 562, 480
 Clayton, D. D., Liu, W., & Dalgarno, A. 1999, *Science*, 283, 1290
 Dalgarno, A., Du, M. L., & You, J. H. 1990, *ApJ*, 349, 675
 Dalgarno, A., Yan, M., & Liu, W. 1999, *ApJS*, 125, 237
 Danziger, I. J., Lucy, L. B., Bouchet, P., & Gouiffes, C. 1991, in *Supernovae, the Tenth Santa Cruz Workshop in Astronomy and Astrophysics*, ed. S. E. Woosley (New York: Springer), 69
 Dwek, E., Galliano, F., & Jones, A. P. 2007, *ApJ*, 662, 927
 Fairbairn, A. R. 1968, *J. Chem. Phys.*, 48, 515
 Fesen, R. A., et al. 2006, *ApJ*, 636, 859
 Fryer, C. L., Woosley, S. E., & Heger, A. 2001, *ApJ*, 550, 371
 Fryxell, B., Arnett, D., & Müller, E. 1991, *ApJ*, 367, 619
 Gearhart, R. A., Wheeler, J. C., & Swartz, D. A. 1999, *ApJ*, 510, 944
 Gerardy, C. L., Fesen, R. A., Höflich, P., & Wheeler, J. C. 2000, *AJ*, 119, 2968
 Hanson, R. K. 1973, *J. Chem. Phys.*, 60, 4970
 Heger, A., & Woosley, S. E. 2002, *ApJ*, 567, 532
 Herant, M., & Benz, W. 1991, *ApJ*, 370, 81
 Itoh, M., Kumagai, S., Shigezuma, T., Nomoto, K., & Nishimura, J. 1987, *Nature*, 330, 233
 Khare, S. P., & Kumar, A., Jr. 1977, *J. Phys. B*, 10, 2239
 Kifonidis, K., Plewa, T., Janka, H.-Th., & Müller, E. 2003, *A&A*, 408, 621
 Kotak, R., et al. 2006, *ApJ*, 651, L117
 Kotak, R., et al. 2009, *ApJ*, submitted
 Kozasa, T., Hasegawa, H., & Nomoto, K. 1989, *ApJ*, 344, 325
 Kozma, C., & Fransson, C. 1992, *ApJ*, 390, 602 (FK92)
 Lepp, S., Dalgarno, A., & McCray, R. 1990, *ApJ*, 358, 262
 Liu, W., & Dalgarno, A. 1994, *ApJ*, 438, 789
 Liu, W., & Dalgarno, A. 1995, *ApJ*, 454, 472
 Liu, W., & Dalgarno, A. 1996, *ApJ*, 471, 480
 Liu, W., Dalgarno, A., & Lepp, S. 1992, *ApJ*, 396, 679
 MacKey, J., Bromm, V., & Hernquist, L. 2003, *ApJ*, 586, 1
 McCray, R. 1993, *ARA&A*, 31, 175
 Meikle, W. P. S., Spyromilio, J., Varani, G.-F., & Allen, D. A. 1989, *MNRAS*, 238, 193
 Müller, E., Fryxell, B., & Arnett, D. 1991, *A&A*, 251, 505
 Nozawa, T., Kozasa, T., Umeda, H., Maeda, K., & Nomoto, K. 2003, *ApJ*, 598, 785 (NK03)
 Nozawa, T., et al. 2007, *ApJ*, 666, 955
 Omukai, K., & Nishi, R. 1998, *ApJ*, 508, 141
 Pei, Y. C., & Fall, S. M. 1995, *ApJ*, 454, 69
 Pettini, M., Smith, L. J., Hunstead, R. W., & King, D. L. 1994, *ApJ*, 426, 79
 Petuchowski, S. J., Dwek, E., Allen, J. E., & Nuth, J. A., III. 1989, *ApJ*, 342, 406
 Pinto, P. A., & Woosley, S. E. 1988, *Nature*, 333, 534
 Pozzo, M., et al. 2006, *MNRAS*, 368, 1169
 Rho, J., Jarrett, T. H., Reach, W. T., Gomez, H., & Andersen, M. 2009, *ApJ*, 693, L39
 Robson, I., Priddey, R. S., Isaak, K. G., & McMahan, R. G. 2004, *MNRAS*, 351, L29
 Roche, P. F., Aitken, D. K., & Smith, C. H. 1991, *MNRAS*, 252, 39
 Schneider, R., Ferrara, A., & Salvaterra, R. 2004, *MNRAS*, 351, 1379 (SFS04)
 Schneider, R., Omukai, K., Inoue, A. K., & Ferrara, A. 2006, *MNRAS*, 369, 1437
 Shigezuma, T., & Nomoto, K. 1990, *ApJ*, 360, 242
 Singh, P. D., & Andreezza, C. M. 2000, *ApJ*, 537, 261
 Smith, J. D., et al. 2009, *ApJ*, 693, 713
 Spyromilio, J., & Leibundgut, B. 1996, *MNRAS*, 283, L89
 Spyromilio, J., Meikle, W. P. S., Learner, R. C. M., & Allen, D. A. 1988, *Nature*, 334, 327
 Sunyaev, R. A., et al. 1990, *Sov. Astron. Lett.*, 16, 171
 Todini, P., & Ferrara, A. 2001, *MNRAS*, 325, 726
 Umeda, H., & Nomoto, K. 2002, *ApJ*, 565, 385 (UN02)
 Willacy, K., & Cherchneff, I. 1998, *A&A*, 330, 676
 Woodall, J., Agúndez, M., Markwick-Kemper, A. J., & Millar, T. J. 2007, *A&A*, 466, 1197
 Wooden, D. H., et al. 1993, *ApJS*, 88, 477
 Woosley, S. E. 1988, *ApJ*, 330, 218
 Woosley, S. E., Pinto, P. A., & Hartmann, D. 1989, *ApJ*, 346, 395
 Zinner, E. 2006, in *Treatise on Geochemistry*, Vol. 1.02, ed. H. D. Holland & K. K. Turekian (Oxford: Elsevier), 1